


GRM2 Regulates Functional Integration of Adult-Born DGCs by Paradoxically Modulating MEK/ERK1/2 Pathway

Jiao Ma,^{1,3*} Zhechun Hu,^{2*} Huimin Yue,^{1,2} Yujian Luo,^{1,2} Chao Wang,² Xuan Wu,³ Yan Gu,^{3,4} and  Lang Wang^{1,2}

¹Department of Neurology of the First Affiliated Hospital, Interdisciplinary Institute of Neuroscience and Technology, Zhejiang University School of Medicine, 310027 Hangzhou, People's Republic of China, ²School of Brain Science and Brain Medicine, Zhejiang University, 310058 Hangzhou, People's Republic of China, ³Center of Stem Cell and Regenerative Medicine, and Department of Neurology of the Second Affiliated Hospital, NHC and CAMS Key Laboratory of Medical Neurobiology, Zhejiang University School of Medicine, 310058 Hangzhou, People's Republic of China, and ⁴MOE Frontier Science Center for Brain Science and Brain-Machine Integration, Zhejiang University, 310058 Hangzhou, People's Republic of China

Metabotropic glutamate receptor 2 (GRM2) is highly expressed in hippocampal dentate granule cells (DGCs), regulating synaptic transmission and hippocampal functions. Newborn DGCs are continuously generated throughout life and express GRM2 when they are mature. However, it remained unclear whether and how GRM2 regulates the development and integration of these newborn neurons. We discovered that the expression of GRM2 in adult-born DGCs increased with neuronal development in mice of both sexes. Lack of GRM2 caused developmental defects of DGCs and impaired hippocampus-dependent cognitive functions. Intriguingly, our data showed that knockdown of *Grm2* resulted in decreased b/c-Raf kinases and paradoxically led to an excessive activation of MEK/ERK1/2 pathway. Inhibition of MEK ameliorated the developmental defects caused by *Grm2* knockdown. Together, our results indicate that GRM2 is necessary for the development and functional integration of newborn DGCs in the adult hippocampus through regulating the phosphorylation and activation state of MEK/ERK1/2 pathway.

Key words: adult neurogenesis; adult-born dentate granule cells; GRM2; hippocampus; MEK/ERK1/2 pathway; object-to-location recognition

Significance Statement

Metabotropic glutamate receptor 2 (GRM2) is highly expressed in mature dentate granule cells (DGCs) in the hippocampus. It remains unclear whether GRM2 is required for the development and integration of adult-born DGCs. We provided *in vivo* and *in vitro* evidence to show that GRM2 regulates the development of adult-born DGCs and their integration into existing hippocampal circuits. Lack of GRM2 in a cohort of newborn DGCs impaired object-to-location memory in mice. Moreover, we revealed that GRM2 knockdown paradoxically upregulated MEK/ERK1/2 pathway by suppressing b/c-Raf in developing neurons, which is likely a common mechanism underlying the regulation of the development of neurons expressing GRM2. Thus, Raf/MEK/ERK1/2 pathway could be a potential target for brain diseases related to GRM2 abnormality.

Introduction

In the hippocampal dentate gyrus (DG) of adult mammals, new neurons are continuously generated throughout life. These

adult-born dentate granule cells (DGCs) integrate into the hippocampal neural circuits and are recruited for coding a variety of memories, as well as regulating mood and emotions (Gonçalves et al., 2016). Correct synaptic integration into the hippocampal neural circuits is essential for proper functions of newborn DGCs, whereas aberrant development and integration are often associated with functional deficits of newborn DGCs in diseases such as schizophrenia, epilepsy, and Alzheimer's disease (Duan et al., 2007; Walter et al., 2007; Sun et al., 2009; Lybrand et al., 2021).

Group II inhibitory metabotropic glutamate receptors (GRMs), consisting of type 2 and 3 GRMs (GRM2/3), are expressed in DGCs, locating on their axon terminals [i.e., mossy fiber (MF) boutons; Shigemoto et al., 1997]. Present on MF terminals targeting CA3 pyramidal cells (Kamiya et al., 1996), CA3 interneurons (Maccaferri et al., 1998), and

Received Oct. 5, 2022; revised Feb. 1, 2023; accepted Feb. 19, 2023.

Author contributions: L.W. designed research; J.M., Z.H., H.Y., Y.L., C.W., X.W., and Y.G. performed research; J.M., Z.H., and H.Y. analyzed data; Y.G. and L.W. wrote the paper.

This work was supported by the National Key R&D Program of China (Grant 2020AAA0105900), the National Natural Science Foundation of China (Grants 32070975 and 32071021), and the Zhejiang Provincial Natural Science Foundation of China (Grant LR21C090001). We thank the Core Facilities of Zhejiang University School of Medicine for technical assistance.

*J.M. and Z.H. contributed equally.

The authors declare no competing financial interests.

Correspondence should be addressed to Lang Wang at wanglang@zju.edu.cn or Yan Gu at guyan2015@zju.edu.cn.

<https://doi.org/10.1523/JNEUROSCI.1886-22.2023>

Copyright © 2023 the authors

hilar interneurons (Doherty and Dingledine, 1998), GRM2/3 in DGCs is important for the regulation of strength and plasticity of MF synapses (Nicholls et al., 2006). Previous studies showed that GRM2/3 and GRM2 exhibit similar immunoreactivity in the MF terminal zone (Shigemoto et al., 1997), and that the GRM2/3 immunoreactivity were almost lost in mice lacking *Grm2* gene (Yokoi et al., 1996), indicating that GRM2 is the major type of group II GRMs expressed in DGCs. Coupled to *Gai*, when activated, GRM2 on MF terminals inhibits cAMP production and protein kinase A (PKA) activity, activates G-protein-coupled inwardly rectifying potassium channels and inhibits voltage-gated calcium channels through $G\beta\gamma$, thus suppressing the presynaptic release of neurotransmitters (Kamiya et al., 1996; Tzounopoulos et al., 1998; Cosgrove et al., 2011). Aberrant expression of GRM2 in CA3 MF terminals has been reported in epileptic animal models (Pacheco Ojalora et al., 2006) and in vulnerable neurons in Alzheimer's disease (Lee et al., 2004), suggesting that the expression of GRM2 in DGCs is necessary for hippocampal functions.

GRM2 is not only expressed in the embryonically born DGCs, but also is expressed in the adult-born DGCs. Previous studies have shown that the transmitter release from the axon terminals of adult-born DGCs could be inhibited by group II GRMs agonists, indicating the expression of GRM2 in adult-born DGCs when they are fully mature and successfully integrated (Toni et al., 2008; Gu et al., 2012). As new neurons are continuously adding to the granule cell population in the DG, the expression of GRM2 in the newly integrated DGCs is likely to be required for the proper function of hippocampal circuits. However, it remains unclear when newborn DGCs start to express GRM2, and whether GRM2 is necessary for the development and integration of newborn DGCs in the adult brain.

In this study, we investigated the function of GRM2 during the development and integration of newborn DGCs in the adult hippocampus. We discovered that the expression of GRM2 in adult-born DGCs increased with development. *Grm2* knock-down suppressed the development and integration of adult-born DGCs by paradoxically upregulating the mitogen-activated protein kinase kinase (MEK)/extracellular signal-regulated protein kinase 1 (ERK1)/ERK 2 signaling pathway and impaired hippocampus-dependent cognitive functions. Inhibition of MEK activity by overexpressing a dominant-negative *Mapk1* (*dnMapk1*) ameliorated the developmental defects caused by *Grm2* knock-down. Together, our results indicate that GRM2 is required for the development and functional integration of newborn DGCs in the adult hippocampus through regulating the phosphorylation and activation state of MEK/ERK pathways.

Materials and Methods

Animals

All procedures were approved by the Animal Care and Use Committees at the Zhejiang University School of Medicine and were conducted in accordance with the policies of institutional guidelines on the care and use of laboratory animals.

Young adult C57BL/6 mice (age, 8–10 weeks) were used in the present research. Mice were bred and group housed in the animal facility of Zhejiang University School of Medicine. Mice were maintained in a 12 h light/dark cycle and had free access to water and food. Both male and female mice were used for experiments.

Primary neuronal culture

Hippocampi were dissected from embryonic day 14.5 mouse embryos and digested in 0.25% trypsin at 37°C for 10 min. DMEM/high-glucose

(catalog #SH30243.01, Hyclone) containing 10% fetal bovine serum (FBS; ES cell qualified; catalog #SE200-ES, VISTECH) was added to terminate the digestion. After washing with Dulbecco's PBS, hippocampal tissues were dissociated into single cells by pipetting with glass Pasteur pipettes. Cells were then filtered through a 40 μ m strainer and plated on coverslips coated with poly-D-lysine (catalog #P0899, Sigma-Aldrich) in DMEM/high-glucose containing 10% FBS. After 30 min, the medium was completely replaced by Neurobasal medium (catalog #21103-049, Thermo Fisher Scientific) supplemented with 2% B27 (catalog #17504-044, Thermo Fisher Scientific), and 1% GlutaMax (catalog #35050-061, Thermo Fisher Scientific). Medium was half-changed every 3 d thereafter, and neurons were used at a preferred time after being cultured *in vitro*.

Construction of viral plasmid vectors

Short hairpin *Grm2* retroviral and lentiviral vectors. Three shRNAs were designed against different regions of mouse *Grm2*, and the one with the best knockdown efficacy was selected for constructing retroviral and lentiviral vectors. A control (Ctrl) shRNA sequence not specific for any known gene was also inserted into the same retroviral and lentiviral vectors.

***dnMapk1* retroviral and lentiviral vectors.** Mouse *Mapk1* mRNA coding sequences were obtained from GenBank (NM_011949.3), synthesized with two point mutations (to change Thr¹⁸⁵ and Tyr¹⁸⁷ to Ala residues in its protein product), and subcloned into retroviral and lentiviral plasmid vectors. In these viral vectors, the expression of *dnMapk1* and dTomato was inducible under the regulation of Tet-responsive element (TRE), as described previously (Kumamoto et al., 2012).

Virus production

As previously described (Hu et al., 2022), each retroviral or lentiviral backbone plasmid was cotransfected to HEK293T cells with helper plasmids for retrovirus or lentivirus using Lipofectamine (catalog #40802ES09, Yeasen). Culture medium was collected, and then the virus was purified and concentrated by ultracentrifugation.

Viral application

Retrovirus was injected into the DG of adult mice. Briefly, mice were anesthetized with isoflurane and placed on a stereotaxic apparatus. After the surgery for craniotomy, viral particles were injected bilaterally into the DG. The coordinates are 2.0 mm caudal to bregma, 1.6 mm lateral from the midline and 2.5 mm ventral from the skull surface; 3.0 mm caudal to bregma, 2.6 mm lateral from the midline and 3.2 mm ventral from the skull surface. After surgery, mice were allowed to recover in a clean cage, and then returned to their home cages.

For the infection of cultured cells using lentivirus, viral particles were applied to cells at 4 d *in vitro* (DIV). Briefly, virus was diluted into culture medium, and polybrene was applied at the same time at a final concentration of 6 μ g/ml. Cells were harvested for Western blotting or fixed for immunostaining at 9 DIV.

Single-cell qRT-PCR

The total RNA was extracted by using the Single Cell-to-CT qRT-PCR (quantitative real-time PCR) Kit (catalog #4458237, Thermo Fisher Scientific). qRT-PCR was performed using the TB Green Premix Ex Taq II (Tli RNaseH Plus; catalog #RR820A, Takara) and a BIO-RAD CFX96 (96-well format). The fold change in mRNA expression of gene was normalized to β -actin using the $\Delta\Delta C_t$ method. The primers used for qRT-PCR were as follows: *Grm2*: 5'-GCTCCCACAGCTATACCG-3' (forward), and 5'-TCATAACGGGACTTGTGCTC-3' (reverse); and *gapdh*: 5'-TGTGTCCGTCGTGGATCTGA-3' (forward), and 5'-TTGCTGTTGAAGTCGCAGGAG-3' (reverse).

Drug administration

For *in vivo* induction of *dnMapk1* expression, doxycycline (Dox; catalog #MB1088, Meilunbio) was administered at a concentration of 2 mg/ml through drinking water with 5% sucrose (w/v). When used on cultured cells, Dox was applied by dissolving in culture medium at a final concentration of 2 μ g/ml, from 5 to 9 DIV.

For the drug treatment of cultured hippocampal neurons, chemicals were dissolved in the culture medium and applied to cells. The final concentrations of DMU-212 (catalog #HY-137977/CS-0143458, MedChemExpress), SB590885 (catalog #S80705, MedMol) and GW5074 (catalog #G129612, Aladdin) was 7.5, 0.2, and 0.5 μM , respectively. For Western blotting, the chemicals were applied to cells from 7 to 9 DIV. For immunostaining, the chemicals were applied to cells from 4 to 9 DIV.

Western blot analysis

To detect the levels of GRM2 and other proteins in the DG, mice were anesthetized with isoflurane, and the brain was removed and cut into 300 μm acute slices in cold PBS. The DG tissues were dissected, homogenized, and centrifuged at 12,000 rpm at 4°C for 15 min. For cultured cells, cells were washed with cold PBS and then lysed in RIPA buffer (catalog #20101ES60, Yeasen) containing EDTA-free protease inhibitors (catalog #4693132001, Roche) and phosphatase inhibitors (catalog #4906837001, Roche) on ice for 10–20 min. The cell lysates were then homogenized and centrifuged at 12,000 rpm at 4°C for 15 min.

The supernatant was then collected and protein concentration was detected by the BCA Protein Assay Kit (catalog #P0011, Beyotime). Samples were diluted in 5 \times loading buffer and were boiled at 100°C for 10 min. Proteins were then separated in 12% gel by SDS-PAGE and transferred to PVDF membranes (catalog #ISEQ00010, Merck Millipore), which were then blocked with 5% nonfat milk in TBST buffer at room temperature for 1 h. Membranes were incubated with primary antibodies to GRM2 (1:500; catalog #SAB4501319, Sigma-Aldrich), phosphorylated ERK1/2 (pERK1/2; 1:1000; catalog #4370s, Cell Signaling Technology), ERK1/2 (1:1000; catalog #9102s, Cell Signaling Technology), MEK (1:1000; catalog #9122s, Cell Signaling Technology), pMEK (1:1000; catalog #9154s, Cell Signaling Technology), cAMP response element-binding protein (CREB; 1:1000; catalog #9197s, Cell Signaling Technology), pCREB (1:1000; catalog #9198s, Cell Signaling Technology), PKA- α (1:1000; catalog #4782s, Cell Signaling Technology), pPKA-C (1:1000; catalog #4781s, Cell Signaling Technology), PSD95 (1:1000; catalog #3450s, Cell Signaling Technology), Homer1 (1:500; catalog #160011, SYSS), L1Cam (1:1000; catalog #Ab24345, Abcam), PKC α (1:1000; catalog #2056s, Cell Signaling Technology), pPKC α/β (1:1000; catalog #9375s, Cell Signaling Technology), c-Raf (1:1000; catalog #9422s, Cell Signaling Technology), or b-Raf (1:2000; catalog #A15033, ABclonal) at 4°C overnight. Membranes were then incubated with horseradish peroxidase-conjugated goat-anti-rabbit IgG (1:5000; Earthox) at room temperature for 1 h. Bands were visualized with the ECL Kit (catalog #34077, Thermo Fisher Scientific) and imaged using the GE AI600 Imaging System. β -Tubulin (1:3000; catalog #30302ES20, Yeasen) was used as an internal control. Quantitative analysis was performed with ImageJ software. All experiments were repeated at least three times.

Immunostaining, confocal imaging, and image analysis

Mice were deeply anesthetized and perfused transcardially with PBS and then 4% paraformaldehyde (PFA). Brains were removed, fixed overnight in PFA, and then transferred to a 30% (w/v) sucrose solution and stored at 4°C. Brains were sectioned into 50 μm coronal sections covering the full anterior–posterior extent of the hippocampus. For cultured hippocampal neurons, cells were fixed with ice-cold 4% PFA solution.

The slices/cells were then permeabilized with 0.2% Triton X-100 and blocked in 5% normal donkey serum. Regular immunostaining was performed using primary antibodies to GRM2 (1:50; catalog #SAB4501319, Sigma-Aldrich), PROX1 (1:500; catalog #ab199359, Abcam), doublecortin (DCX; 1:1000; catalog #4604, Cell Signaling Technology), MAP2 (1:2000; catalog #M1406, Sigma-Aldrich), RFP (1:2000; catalog #Ab62341, Abcam), or green fluorescent protein (GFP; 1:3000; catalog #ab13970, Abcam), overnight at 4°C, followed by incubation with secondary antibodies [Cy2-conjugated donkey antibody to chicken (1:1000; catalog #703–225-155, Jackson ImmunoResearch), Cy3-conjugated donkey antibody to rabbit (1:1000; catalog #711–165-152, Jackson ImmunoResearch), Cy5-conjugated donkey antibody to rabbit (1:1000; catalog #711–175-152, Jackson ImmunoResearch), or Cy5-conjugated donkey antibody to chicken (1:1000; catalog #703–175-155, Jackson ImmunoResearch)] for 2 h at room temperature (25°C), in the

presence of 2% donkey serum, 1% bovine serum albumin, and 0.2% (w/v) Triton X-100. Sections were mounted on slides with Fluoromount-G anti-fade medium containing DAPI (catalog #0100–20, SouthernBiotech). Images of z series stacks were taken on a confocal microscope (model FV3000, Olympus). Images were analyzed using ImageJ or Imaris software.

RNAscope in situ hybridization

Brain slices (14 μm) were prepared from PFA-fixed brain tissue. Ethanol was used for gradient dehydration of the sections. Probes were designed by ACDbio (probes: Mm-Grm2, catalog #317831; Neg-ctrl, catalog #320871; Pos-ctrl, catalog #320881). *In situ* hybridization was then performed using RNAscope multiplex fluorescent reagent kit (Advanced Cell Diagnostics) according to standard instructions from the manufacturer. Additional immunostaining was performed following the detection of mRNA with standard protocols, as described above. Images were accessed with an confocal microscope (FV3000, Olympus). For quantification, images were analyzed using ImageJ.

Electrophysiological recording

Acute brain sections were made 3 weeks after retroviral injection, and electrophysiological recordings were performed at 32–34°C, as previously described (Hu et al., 2022). Briefly, mice were deeply anesthetized with isoflurane, and brain was removed and acute brain slices were prepared. GFP-labeled neurons were identified under fluorescent microscope and whole-cell patch-clamp recordings were performed. The intrinsic properties and action potentials (APs) of the neurons were recorded in regular ACSF. Miniature EPSCs (mEPSCs) were recorded in the presence of tetrodotoxin (1 μM) and picrotoxin (100 μM) at a holding potential of -70 mV. Miniature events were automatically detected and then analyzed using Clampfit software.

Behavioral tests

Open field. Mice were placed in a brightly illuminated open field (45 \times 45 cm) and allowed to freely explore the space for 10 min. Movement and position of the mice were recorded by an overhead camera. The open field was divided into the outer zone and the inner zone. The total travel distance and the percentage of time that the mice spent in each zone were measured by the software.

Novel location and novel object recognition tests. For the novel location recognition test, mice were placed in a normally illuminated box (45 \times 45 cm) with an overhead camera, were allowed to habituate for 10 min, and then put back into the home cage. One hour later, two identical objects were placed close to two corners in the box; mice were put into the box and allowed to freely explore for 10 min. Another hour later, before the test session, one of the two identical objects was placed at a different location (novel location), while the other object was not moved; mice were put back in the box for 10 min, and the time of their exploration on the two objects was recorded and analyzed.

For the novel object recognition test, mice were placed in a normally illuminated box (45 \times 45 cm) with an overhead camera, allowed to habituate for 10 min, and then put back into the home cage. One hour later, two identical objects were placed close to two corners in the box; mice were put into the box and allowed to freely explore for 10 min. Another hour later, before the test session, one of the two identical objects was replaced with a different object (novel object), while the other object was not changed or moved; mice were put back in the box for 10 min, and the time of their exploration of the two objects was recorded and analyzed.

Elevated plus-maze test. Mice were placed in the center of an elevated plus-maze with opposite open and closed arms and allowed to freely explore the maze for 10 min. The behavior and position of each animal were recorded by an overhead camera. The number of entrances and the percentage of time spent in open and closed arms by each animal were measured by the software.

Contextual fear conditioning and test. As previously described (Hu et al., 2022), mice were trained in a conditioning chamber (18 \times 18 \times 30 cm; Coulbourn), containing a stainless steel shock-grid floor. During the training, mice were placed in the chamber and received a single footshock (0.75 mA; duration, 2 s) after 2 min. Mice were taken out of the training

chamber 1 min after the footshock and placed back into their home cages. After training, mice were housed under standard conditions with a 12 h light/dark cycle until the test. Twenty-four hours later, mice were placed back into the same chamber for 5 min, without footshock. Freezing behavior of the mice was monitored via overhead cameras and was measured by an automated scoring system.

Experimental design and statistical analysis

Data are presented as the mean \pm SEM. Statistical analysis was performed using GraphPad Prism 8.0 software. Pooled data were analyzed by two-tailed unpaired *t* tests or otherwise indicated in the figure legends. For box-and-whisker plots, whiskers represent the minimum and maximum, the box represents the upper and lower quartiles, the line in the middle represents the median, and the “+” symbol represents the mean. Statistical significance was considered when $p < 0.05$.

Results

GRM2 is required for the development of newborn DGCs

Previous studies have shown that GRM2 is highly expressed in the hippocampal DG (Shigemoto et al., 1997). To specifically verify the expression of GRM2 in the DG, we used RNAscope, a highly sensitive fluorescent *in situ* hybridization method, and found that, when comparison was made with the large quantity of dots in PROX1⁺ mature DGCs (Fig. 1A), the newborn DGCs expressing DCX showed significantly fewer dots (Fig. 1B,C), suggesting an initially low expression level of *Grm2* after the birth of the new neurons. To determine the change of *Grm2* expression in the adult-born DGCs with their development, we infused engineered murine retrovirus into adult C57BL/6 mice to label the newborn neurons by expressing GFP, then extracted the cells at 1, 2, 3, 4, and 8 weeks post-virus injection (wpi), and performed single-cell qRT-PCR to examine the expression level of *Grm2* mRNAs (Fig. 1D). We found that the expression of *Grm2* increased with the development of newborn neurons and reached a comparable level with 8-week-old mature DGCs when these new neurons were at 3 weeks of age (Fig. 1E), suggesting an increase of *Grm2* expression level with neuronal maturation.

To examine whether GRM2 plays any essential role during the development of newborn DGCs, we next constructed a lentiviral vector to express an shRNA to knock down the expression of endogenous *Grm2* (sh*Grm2*), while using a Ctrl shRNA against a scrambled sequence. After infecting cultured hippocampal neurons with the viruses, we confirmed that sh*Grm2* could efficiently knock down the level of endogenous GRM2 to ~10% (Fig. 1F,G) and therefore significantly decrease the immunoreactivity of GRM2 in these cultured neurons (Fig. 1H,I).

We next constructed sh*Grm2* and Ctrl retroviral vectors and injected the retrovirus into the DG of 8-week-old mice to label the newborn DGCs with GFP. We analyzed the development of newborn DGCs from 1 through 8 wpi (Fig. 1J) and found that the decrease of GRM2 reduced both the total length of dendrites and the number of dendritic branches from 2 weeks on after birth (Fig. 1K,L), thus reducing the complexity of the dendritic arborization of the newborn DGCs (Fig. 1M). To verify these results, we cultured hippocampal neurons *in vitro* and infected the neurons with lentivirus to knock down *Grm2* (Fig. 1N). Consistently, *Grm2* knockdown significantly decreased the dendritic complexity, the total length, and the number of neurites in cultured neurons (Fig. 1O–Q).

To examine whether the intrinsic electrophysiological properties of the newborn DGCs were altered by *Grm2* knockdown, we performed whole-cell patch-clamp recordings in control and sh*Grm2* newborn neurons in acute brain slices at 3 wpi. We found that sh*Grm2* neurons showed significantly increased

membrane resistance and decreased membrane capacitance, compared with Ctrl neurons (Fig. 2A,B). Under current-clamp mode, we found that *Grm2* knockdown did not alter the resting membrane potential of the newborn neurons (Fig. 2C,D). The sh*Grm2* neurons showed similar AP firing compared with Ctrl neurons when small currents were injected, but showed fewer APs in response to large current injections (Fig. 2C,E). The action potential of sh*Grm2* neurons exhibited a similar amplitude but a larger half-width, compared with that of Ctrl neurons (Fig. 2F,G). These differences in the intrinsic properties suggest that the sh*Grm2* neurons were less mature than Ctrl neurons, consistent with the morphologic changes of these neurons.

These results suggest that proper expression of GRM2 is essential for neuronal development.

GRM2 is necessary for proper synaptic integration of newborn DGCs

To further find out whether *Grm2* knockdown leads to abnormal functional integration of the newborn neurons, along with their morphologic defects, we then examined the dendritic spines in the newborn DGCs at 3 wpi (Fig. 3A). We found that *Grm2* knockdown significantly reduced the number of different types of spines, including thin, stubby, and mushroom spines (Fig. 3B), thus decreasing the overall spine density in the newborn DGCs (Fig. 3C). Furthermore, to assess the functional synapse formation onto the newborn DGCs, we recorded the mEPSCs in control and sh*Grm2* newborn neurons in acute brain slices at 3 wpi (Fig. 3D). Our results showed that *Grm2* knockdown significantly decreased the frequency of mEPSCs, without altering their amplitude (Fig. 3E–H), consistent with the decreased spine density in these neurons, suggesting an impaired dendritic integration. To test whether *Grm2* knockdown may also alter the axonal integration of the newborn neurons, we examined the axon boutons from the newborn DGCs at 4 wpi. We found the newborn DGCs with *Grm2* knockdown showed significantly decreased bouton size (Fig. 3I,J), suggesting that *Grm2* knockdown also hindered the axonal integration of the new neurons. On the other hand, *Grm2* knockdown increased the colocalization of activated Caspase 3 (aCasp3) and the newborn DGCs specifically at 3 wpi (Fig. 3K,L), suggesting that the lack of GRM2 enhanced the apoptosis of newborn DGCs specifically during their circuit integration.

In addition, in cultured hippocampal neurons, we found that knockdown of *Grm2* significantly decreased the level of synaptic proteins, such as Homer1, PSD95 and L1cam (Fig. 3M–Q), confirming that knockdown of GRM2 impaired the growth and synapse formation of the newborn neurons.

Together, these results suggest that GRM2 is necessary not only for the morphologic development, but also for the formation of synapses and functional integration of newborn neurons. The failed integration will further lead to the death of newborn DGCs.

Grm2 knockdown led to ERK1/2 phosphorylation and nuclear translocation

To find out possible downstream mechanisms, we examined the level of molecules that may regulate cell development, CREB (Merz et al., 2011) and ERK1/2 (Kim et al., 2004). In cultured hippocampal neurons, *Grm2* knockdown did not affect the total protein level of CREB or pCREB (Fig. 4A,B). However, *Grm2* knockdown significantly increased the pERK1/2, without affecting the total amount of ERK1/2 (Fig. 4A,C). Furthermore, after

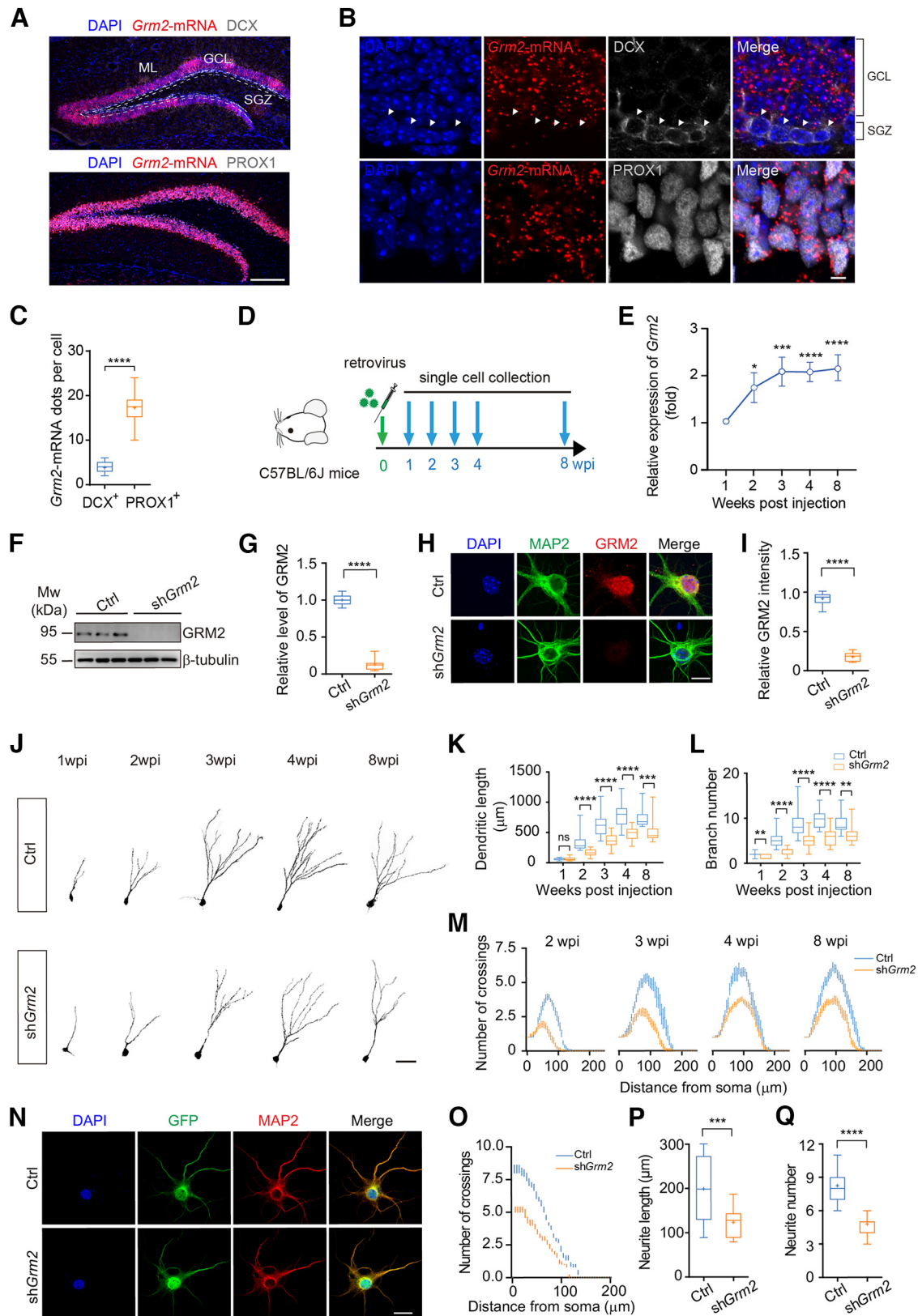


Figure 1. GRM2 is required for the development of newborn DGCs. **A**, Images showing *Grm2* mRNA with immunostaining of DCX (top) or PROX1 (bottom) in the DG. Scale bar, 200 μ m. **B**, Zoom-in images showing the colocalization of *Grm2* mRNA with DCX⁺ cells (top, white arrowheads) and PROX1⁺ cells (bottom). Scale bar, 10 μ m. **C**, *Grm2* mRNA dots per cell in DCX⁺ cells and PROX1⁺ cells (DCX⁺: $N = 3$ mice, $n = 40$ cells; PROX1⁺: $N = 3$ mice, $n = 48$ cells; unpaired t test, $t_{(86)} = 25.27$, **** $p < 0.0001$). **D**, Schematics showing viral labeling and single-cell collection of newborn DGCs. **E**, qRT-PCR showing the relative expression of *Grm2* in newborn DGCs at different time points ($N = 3$ mice, $n = 64$ cells for each time point; unpaired t test; 2 vs 1 wpi: $t_{(126)} = 2.282$, * $p = 0.0241$; 3 vs 1 wpi: $t_{(126)} = 3.448$, *** $p = 0.0008$; 4 vs 1 wpi: $t_{(126)} = 5.11$, **** $p < 0.0001$; 8 vs 1 wpi: $t_{(126)} = 4.08$, **** $p < 0.0001$). **F**, Western blots showing shGrm2 lentivirus decreased GRM2 protein level in cultured hippocampal neurons. **G**, *Grm2* knockdown decreased GRM2 protein level in cultured hippocampal neurons (Ctrl, $n = 6$; shGrm2, $n = 6$; unpaired t test, $t_{(24)} = 28.68$, **** $p < 0.0001$). **H**, Images showing the immunostaining of GRM2 in cultured hippocampal neurons treated with Ctrl (top) or shGrm2 (bottom) viruses. **I**, Relative GRM2 intensity in cultured hippocampal neurons treated with Ctrl (top) or shGrm2 (bottom) viruses. **** $p < 0.0001$. **J**, Representative images of dendritic development in newborn DGCs at 1, 2, 3, 4, and 8 wpi in Ctrl (top) and shGrm2 (bottom) groups. Scale bar, 100 μ m. **K**, Box plots showing dendritic length in newborn DGCs at 1, 2, 3, 4, and 8 wpi in Ctrl (blue) and shGrm2 (orange) groups. **** $p < 0.0001$, ns = not significant. **L**, Box plots showing branch number in newborn DGCs at 1, 2, 3, 4, and 8 wpi in Ctrl (blue) and shGrm2 (orange) groups. **** $p < 0.0001$. **M**, Line graphs showing the number of crossings in newborn DGCs at 2, 3, 4, and 8 wpi in Ctrl (blue) and shGrm2 (orange) groups. **** $p < 0.0001$. **N**, Representative images of cultured hippocampal neurons treated with Ctrl (top) or shGrm2 (bottom) viruses. Scale bar, 10 μ m. **O**, Line graphs showing the number of crossings in cultured hippocampal neurons treated with Ctrl (blue) or shGrm2 (orange) viruses. **** $p < 0.0001$. **P**, Box plots showing neurite length in cultured hippocampal neurons treated with Ctrl (blue) or shGrm2 (orange) viruses. *** $p < 0.001$. **Q**, Box plots showing neurite number in cultured hippocampal neurons treated with Ctrl (blue) or shGrm2 (orange) viruses. **** $p < 0.0001$.

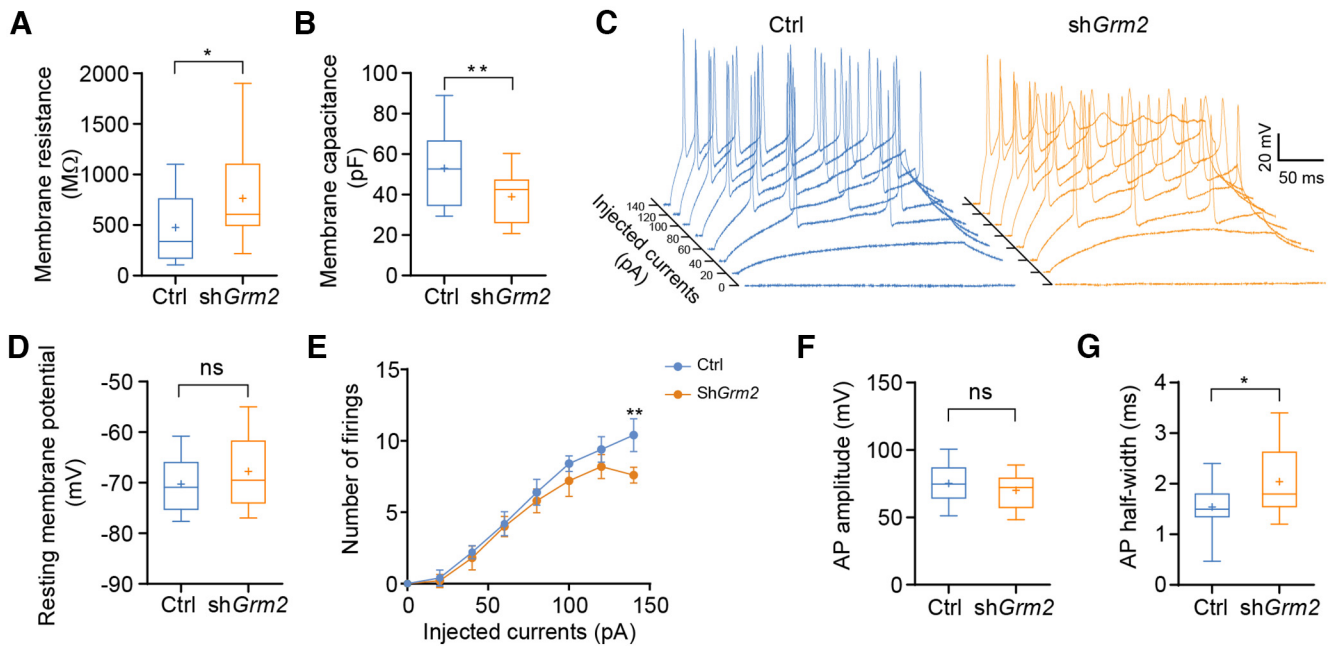


Figure 2. *Grm2* knockdown hindered the maturation of the intrinsic electrophysiological properties of newborn DGs. **A**, *Grm2* knockdown increased the membrane resistance of the adult-born DGs at 3 wpi (Ctrl: *N* = 3 mice, *n* = 17 cells; sh*Grm2*: *N* = 4 mice, *n* = 23 cells; unpaired *t* test, $t_{(38)} = 2.324$, $*p = 0.0256$). **B**, *Grm2* knockdown decreased the membrane capacitance of the adult-born DGs at 3 wpi (Ctrl: *N* = 3 mice, *n* = 17 cells; sh*Grm2*: *N* = 4 mice, *n* = 23 cells; unpaired *t* test, $t_{(38)} = 2.948$, $**p = 0.0054$). **C**, Representative traces recorded from Ctrl and sh*Grm2* adult-born DGs when a series of depolarizing currents were injected. **D**, *Grm2* knockdown did not alter the resting membrane potential of the adult-born DGs at 3 wpi (Ctrl: *N* = 3 mice, *n* = 14 cells; sh*Grm2*: *N* = 4 mice, *n* = 19 cells; unpaired *t* test, $t_{(31)} = 1.092$, $p = 0.2833$). **E**, *Grm2* knockdown decreased the number of firings at large current injection (Ctrl: *N* = 2 mice, *n* = 5 cells; sh*Grm2*: *N* = 2 mice, *n* = 5 cells; unpaired *t* test; when current injection = 140 pA: $t_{(8)} = 4.950$, $**p = 0.0011$). **F**, *Grm2* knockdown did not change the AP amplitude of the adult-born DGs at 3 wpi (Ctrl: *N* = 3 mice, *n* = 15 cells; sh*Grm2*: *N* = 4 mice, *n* = 20 cells; unpaired *t* test, $t_{(33)} = 1.140$, $p = 0.2626$). **G**, *Grm2* knockdown increased the AP half-width of the adult-born DGs (Ctrl: *N* = 3 mice, *n* = 16 cells; sh*Grm2*: *N* = 4 mice, *n* = 22 cells; unpaired *t* test, $t_{(36)} = 2.658$, $*p = 0.0117$).

Grm2 knockdown, we observed an accumulation of pERK1/2 in the nuclei of cultured hippocampal neurons (Fig. 4D,E), suggesting an increased nuclear translocation of phosphorylated ERK1/2 associated with *Grm2* knockdown. We also examined the pERK1/2 level in newborn DGs at 3 wpi by immunostaining and found that the newborn DGs with *Grm2* knockdown

exhibited significantly elevated pERK1/2 levels (Fig. 4F,G). These results suggest that *Grm2* knockdown leads to elevated pERK1/2 in developing neurons.

ERK1/2 is phosphorylated and activated by its upstream kinase, MEK (Wang and Mao, 2019). We then examined the level of both total and pMEK in cultured neurons, and found *Grm2* knockdown significantly increased the level of pMEK, but not the total MEK (Fig. 4H,I).

To verify that the neuronal developmental defects caused by *Grm2* knockdown is related to the upregulated phosphorylation level of MEK/ERK1/2, we then treated cultured hippocampal neurons with DMU-212, which is reported to be able to activate ERK1/2 (Androutsopoulos et al., 2015). We found that DMU-212 treatment significantly increased the levels of both pMEK and pERK1/2 in cultured hippocampal neurons without changing the total amount of MEK and ERK1/2 (Fig. 4J–L), and increased the accumulation of pERK1/2 in the nuclei of these neurons (Fig. 4M,N). Simultaneously, DMU-212 treatment decreased the complexity, total length, and number of neurites in these neurons (Fig. 4O–R), suggesting an impaired neuronal development, consistent with the *Grm2* knockdown-induced neuronal developmental defects. Thus, these data suggest that GRM2 regulates neuronal growth by suppressing ERK1/2 phosphorylation and nuclear translocation.

***Grm2* knockdown paradoxically increased MEK/ERK1/2 phosphorylation by inhibiting b/c-Raf**

To find out how GRM2 regulates MEK/ERK1/2 signaling during neuronal development, we next examined the levels of several proteins that are associated with MEK/ERK1/2 signaling, such as PKC, PKA, and b/c-Raf.

Scale bar, 10 μ m. **I**, *Grm2* knockdown decreased GRM2 immunofluorescence intensity in cultured hippocampal neurons (Ctrl, *n* = 8 cells; sh*Grm2*, *n* = 10 cells; unpaired *t* test, $t_{(31)} = 31.97$, $****p < 0.0001$). **J**, Images showing the dendritic morphology of newborn DGs at different time points after retroviral injection. Scale bar, 50 μ m. **K**, *Grm2* knockdown decreased dendritic length of newborn DGs (unpaired *t* test; 1 wpi: Ctrl: *N* = 3 mice, *n* = 17 cells; sh*Grm2*: *N* = 3 mice, *n* = 20 cells; $t_{(35)} = 0.4626$, $p = 0.6465$; 2 wpi: Ctrl: *N* = 4 mice, *n* = 44 cells; sh*Grm2*: *N* = 3 mice, *n* = 21 cells; $t_{(63)} = 5.941$, $****p < 0.0001$; 3 wpi: Ctrl: *N* = 4 mice, *n* = 34 cells; sh*Grm2*: *N* = 3 mice, *n* = 26 cells; $t_{(58)} = 6.339$, $****p < 0.0001$; 4 wpi: Ctrl: *N* = 3 mice, *n* = 17 cells; sh*Grm2*: *N* = 4 mice, *n* = 28 cells; $t_{(43)} = 6.619$, $****p < 0.0001$; 8 wpi: Ctrl: *N* = 3 mice, *n* = 17 cells; sh*Grm2*: *N* = 3 mice, *n* = 17 cells; $t_{(32)} = 4.254$, $***p = 0.0002$). **L**, *Grm2* knockdown decreased dendritic branch number of newborn DGs (unpaired *t* test, 1 wpi: Ctrl: *N* = 3 mice, *n* = 17 cells; sh*Grm2*: *N* = 3 mice, *n* = 20 cells; $t_{(35)} = 3.488$, $**p = 0.0013$; 2 wpi: Ctrl: *N* = 4 mice, *n* = 44 cells; sh*Grm2*: *N* = 3 mice, *n* = 21 cells; $t_{(63)} = 7.681$, $****p < 0.0001$; 3 wpi: Ctrl: *N* = 4 mice, *n* = 34 cells; sh*Grm2*: *N* = 3 mice, *n* = 26 cells; $t_{(58)} = 6.136$, $****p < 0.0001$; 4 wpi: Ctrl: *N* = 3 mice, *n* = 17 cells; sh*Grm2*: *N* = 4 mice, *n* = 28 cells; $t_{(44)} = 5.765$, $****p < 0.0001$; 8 wpi: Ctrl: *N* = 3 mice, *n* = 17 cells; sh*Grm2*: *N* = 3 mice, *n* = 17 cells; $t_{(32)} = 3.399$, $**p = 0.0018$). **M**, Sholl analysis of newborn neuron dendritic complexity at 2, 3, 4, and 8 weeks after Ctrl or sh*Grm2* retroviral injection. **N**, Images showing the morphology of cultured hippocampal neurons treated with Ctrl and sh*Grm2* viruses. Scale bar, 20 μ m. **O**, Sholl analysis of cultured hippocampal neurons infected with Ctrl and sh*Grm2* viruses. **P**, *Grm2* knockdown reduced the neurite length of cultured hippocampal neurons (Ctrl, *n* = 25 cells; sh*Grm2*, *n* = 19 cells; unpaired *t* test; $t_{(42)} = 4.298$, $***p = 0.0001$). **Q**, *Grm2* knockdown reduced the neurite number of cultured hippocampal neurons (Ctrl, *n* = 20 cells; sh*Grm2*, *n* = 20 cells; unpaired *t* test; $t_{(38)} = 9.815$, $****p < 0.0001$).

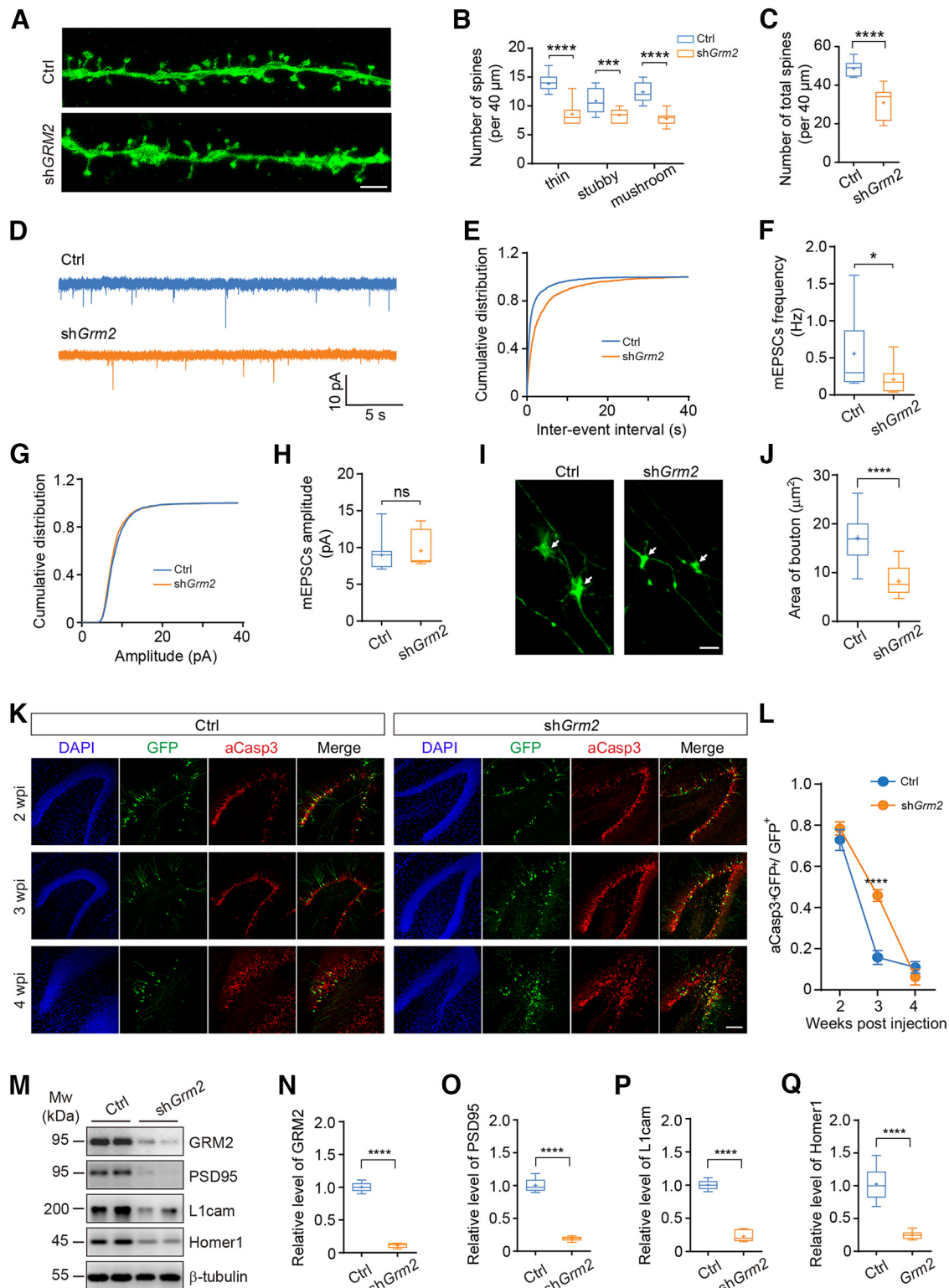


Figure 3. GRM2 is necessary for proper synaptic integration of newborn DGCs. **A**, Confocal images showing the dendritic spines of newborn DGCs at 3 weeks after retroviral injection. Scale bar, 2 μm . **B**, *Grm2* knockdown decreased the density of thin, stubby, and mushroom spines in newborn DGCs at 3 wpi (Ctrl: $N = 3$ mice, $n = 14$ dendritic segments; *shGrm2*: $N = 3$ mice, $n = 14$ dendritic segments; unpaired t test; thin: $t_{(26)} = 8.835$, **** $p < 0.0001$; stubby: $t_{(26)} = 4.123$, **** $p = 0.0003$; mushroom: $t_{(26)} = 9.061$, **** $p < 0.0001$). **C**, *Grm2* knockdown decreased the total spine density of newborn DGCs at 3 wpi (Ctrl: $N = 3$ mice, $n = 14$ dendritic segments; *shGrm2*: $N = 3$ mice, $n = 14$ dendritic segments; unpaired t test, $t_{(26)} = 7.688$, **** $p < 0.0001$). **D**, Representative traces of mEPSCs recorded from newborn DGCs labeled with Ctrl (top) or *shGrm2* (bottom) retroviruses. **E**, Cumulative distribution of interevent intervals of mEPSCs recorded in newborn DGCs (Ctrl: $N = 3$ mice, $n = 7$ cells; *shGrm2*: $N = 3$ mice, $n = 13$ cells; Kolmogorov–Smirnov test, **** $p < 0.0001$). **F**, Average frequency of mEPSCs recorded in newborn DGCs (Ctrl: $N = 3$ mice, $n = 7$ cells; *shGrm2*: $N = 3$ mice, $n = 13$ cells; unpaired t test, $t_{(18)} = 2.205$, * $p = 0.0407$). **G**, Cumulative distribution of mEPSC amplitude of newborn DGCs (Ctrl: $N = 3$ mice, $n = 7$ cells; *shGrm2*: $N = 3$ mice, $n = 13$ cells; Kolmogorov–Smirnov test, $p = 0.8225$). **H**, Average amplitude of mEPSCs recorded in newborn DGCs labeled with Ctrl or *shGrm2* viruses (Ctrl: $N = 3$ mice, $n = 7$ cells; *shGrm2*: $N = 3$ mice, $n = 13$ cells; unpaired t test, $t_{(18)} = 0.545$, $p = 0.5924$). **I**, Confocal images showing the axon boutons (indicated by white arrows) of newborn DGCs at 4 wpi. Scale bar, 5 μm . **J**, *Grm2* knockdown decreased the size of axon boutons of the adult-born DGCs (Ctrl: $N = 2$ mice, $n = 18$ boutons; *shGrm2*: $N = 2$ mice, $n = 18$ boutons; unpaired t test, $t_{(18)} = 4.123$, **** $p = 0.0003$).

Previous studies reported that GRM2 activation in neurons inhibits the production of cAMP, thus suppressing the activity of PKA (Kamiya et al., 1996; Tzounopoulos et al., 1998; Cosgrove et al., 2011). Intriguingly, knockdown of GRM2 did not alter the level of either total PKA-C α or the pPKA-C α (Fig. 5A,B). In the contrary, *Grm2* knockdown decreased the level of both pPKC α / β II and total PKC α (Fig. 5A,C). Simultaneously, knockdown of GRM2 decreased both b-Raf and c-Raf in cultured hippocampal neurons (Fig. 5A,D). Although in most cases the activation of b/c-Raf activates the MEK/ERK1/2 pathway, transactivation of dimerized b/c-Raf could be achieved by Raf inhibitors (Poulikakos et al., 2010; Poulikakos and Rosen, 2011). To certify whether inhibiting b/c-Raf could activate MEK/ERK1/2 signaling, we applied the selective b-Raf inhibitor SB590885 (Jin et al., 2017) or c-Raf inhibitor GW5074 (Chin et al., 2004) on cultured hippocampal neurons. Indeed, we found elevated levels of phosphorylated MEK (Fig. 5E, F) and phosphorylated ERK1/2 (Fig. 5E,G) in the neurons treated with b/c-Raf inhibitors, indicating that inhibited b/c-Raf directly enhanced the activation of the MEK/ERK1/2 signaling pathway. To confirm that Raf inhibitor-induced activation of MEK/ERK1/2 pathway is related to neuronal development, we further examined the neurite morphology of the cultured neurons following the treatment of SB590885. We found that 5 d of SB590885 treatment indeed inhibited the development of neurons, resulting in simpler neurite complexity, smaller neurite number, and shorter neurite length (Fig. 5H–K). These data suggest that GRM2 modulates the Raf/MEK/ERK1/2 pathway in a paradoxical manner, thus regulating neuronal development.

Inhibiting MEK rescues *Grm2* knockdown-induced developmental defects of neurons

Next, to examine whether the excessive activation of MEK/ERK1/2 pathway mediates the *Grm2* knockdown-induced neuronal developmental defects, we constructed a lentiviral vector expressing a dominant-negative form of mouse *Mapk1* gene (*dnMapk1*; Fig. 6A), which encodes the ERK2 protein but with point mutations to switch the phosphorylation sites Thr¹⁸⁵ and Tyr¹⁸⁷ to Ala residues in its protein product. When ectopically expressed, the protein product of this mutant *dnMapk1* could function as an inhibitor of MEK. In cells infected by this virus, the expression of the *dnMapk1* was inducible under the regulation of TRE (Kumamoto et al., 2012). As expected, the expression of *dnMapk1* in the presence of Dox decreased the level of pERK1/2 in HEK293 cells (Fig. 6B,C). We then treated cultured

hippocampal neurons with Dox to induce the expression of *dnMapk1* after coinfection of the neurons with the *shGrm2* and *dnMapk1* lentiviruses (Fig. 6D). We found the expression of *dnMapk1* prevented the translocation of pERK1/2 into the nuclei of these neurons (Fig. 6E,F).

To test whether *dnMapk1* could rescue the *Grm2* knockdown-induced developmental defects of newborn neurons *in vivo*, we coinjected the *dnMapk1* retrovirus and the *shGrm2* retrovirus into the DGs of adult mice (Fig. 6G). We started treating the mice with Dox in drinking water 10 d after viral injection (Fig. 6H), a time when the retrovirus-labeled newborn DGs were experiencing the development and integration of dendrites and axons (Gu et al., 2012; Kumamoto et al., 2012). Also, we could avoid any possible confounding effects resulting from altered proliferation or differentiation caused by ectopic expression of *dnMapk1* (Kao et al., 2001; Tsao et al., 2013). Dox treatment induced the expression of *dnMapk1* and dTomato in virus-labeled newborn DGs (Fig. 6I). We then analyzed the morphology of the GFP⁺ or the GFP⁺dTomato⁺ newborn DGs at 3 wpi and found that the expression of *dnMapk1* rescued the developmental defects of newborn neurons caused by *Grm2* knockdown, with the GFP⁺dTomato⁺ neurons showing normal dendritic length and arborization (Fig. 6J,K). These data indicate that blocking the excessive activation of the MEK/ERK1/2 pathway could prevent the GRM2 knockdown-induced neuronal developmental defects, suggesting that the timely increasing expression of GRM2 after the birth of the newborn DGs is necessary for the normal development and integration of these new neurons via suppressing the MEK/ERK1/2 pathway.

Grm2 knockdown in adult-born DGs impaired object-to-place recognition

Young adult-born DGs are involved in varieties of hippocampus-dependent cognition (Gonçalves et al., 2016). To test whether lack of GRM2 specifically in young newborn DGs may alter hippocampal functions, we made three retroviral injections at an interval of 5 d to knock down *Grm2* from cohorts of newborn neurons. Four weeks after the last injection, we tested the animals in several behavioral paradigms. We found the mice that received *shGrm2* retroviral injections showed similar travel distances and time spent in the central zone in the open field tests, compared with the Ctrl mice (Fig. 7A). There was no significant difference in the number of entries to the open arms or the time spent in the open arms in the elevated plus maze tests between the *shGrm2* and Ctrl animals (Fig. 7B). These data suggest that lack of GRM2 in young adult-born DGs does not affect the locomotion or anxiety levels of the animals.

Furthermore, in contextual fear memory test, there was no significant difference between the freezing time of the *shGrm2* and Ctrl animals during the test session, 24 h after training (Fig. 7C). In the novel object recognition tests, *Grm2* knockdown from young newborn DGs did not alter the preference of the mice toward the novel object (Fig. 7D). However, *Grm2* knockdown from young newborn DGs diminished the preference of the mice toward the object at a new location (Fig. 7E), indicating that a lack of GRM2 in young newborn DGs selectively impaired object-to-place recognition.

To verify whether *dnMapk1* could rescue the cognitive deficits caused by lack of GRM2 in newborn DGs, we coinjected the *shGrm2* and *dnMapk1* retroviruses into the DG of adult wild-type mice. To avoid possible confounding effects of *dnMapk1* on cell proliferation, differentiation, or synaptic

←

n = 24 boutons; unpaired *t* test, $t_{(40)} = 7.614$, *****p* < 0.0001). **K**, Images showing the colocalization of aCasp3 with virally labeled newborn DGs at 2, 3, and 4 wpi. Scale bar, 100 μ m. **L**, The proportion of aCasp3⁺GFP⁺ cells in GFP⁺ newborn DGs at 2, 3, and 4 wpi (2 wpi: Ctrl: *N* = 3 mice, *n* = 12 slices; *shGrm2*: *N* = 4 mice, *n* = 22 slices; unpaired *t* test, $t_{(32)} = 2.022$, *p* = 0.0517; 3 wpi: Ctrl: *N* = 3 mice, *n* = 10 slices; *shGrm2*: *N* = 3 mice, *n* = 11 slices; unpaired *t* test, $t_{19} = 9.04$, *****p* < 0.0001; 4 wpi: Ctrl: *N* = 3 mice, *n* = 13 slices; *shGrm2*: *N* = 2 mice, *n* = 5 slices; unpaired *t* test, $t_{(16)} = 1.034$, *p* = 0.3163). **M**, Western blots showing *Grm2* knockdown decreased the expression of PSD95, L1cam, and Homer1 in cultured hippocampal neurons. **N**, *shGrm2* virus decreased the relative level of GRM2 in cultured hippocampal neurons (Ctrl, *n* = 9; *shGrm2*, *n* = 9; unpaired *t* test, $t_{(16)} = 34.44$, *****p* < 0.0001). **O**, *Grm2* knockdown decreased the relative level of PSD95 in cultured hippocampal neurons (Ctrl, *n* = 6; *shGrm2*, *n* = 6; unpaired *t* test, $t_{(10)} = 18.45$, *****p* < 0.0001). **P**, *Grm2* knockdown decreased the relative level of L1cam in cultured hippocampal neurons (Ctrl, *n* = 9; *shGrm2*, *n* = 9; unpaired *t* test, $t_{(16)} = 21.49$, *****p* < 0.0001). **Q**, *Grm2* knockdown decreased the relative level of Homer1 in cultured hippocampal neurons (Ctrl, *n* = 9; *shGrm2*, *n* = 9; unpaired *t* test, $t_{(16)} = 9.441$, *****p* < 0.0001).

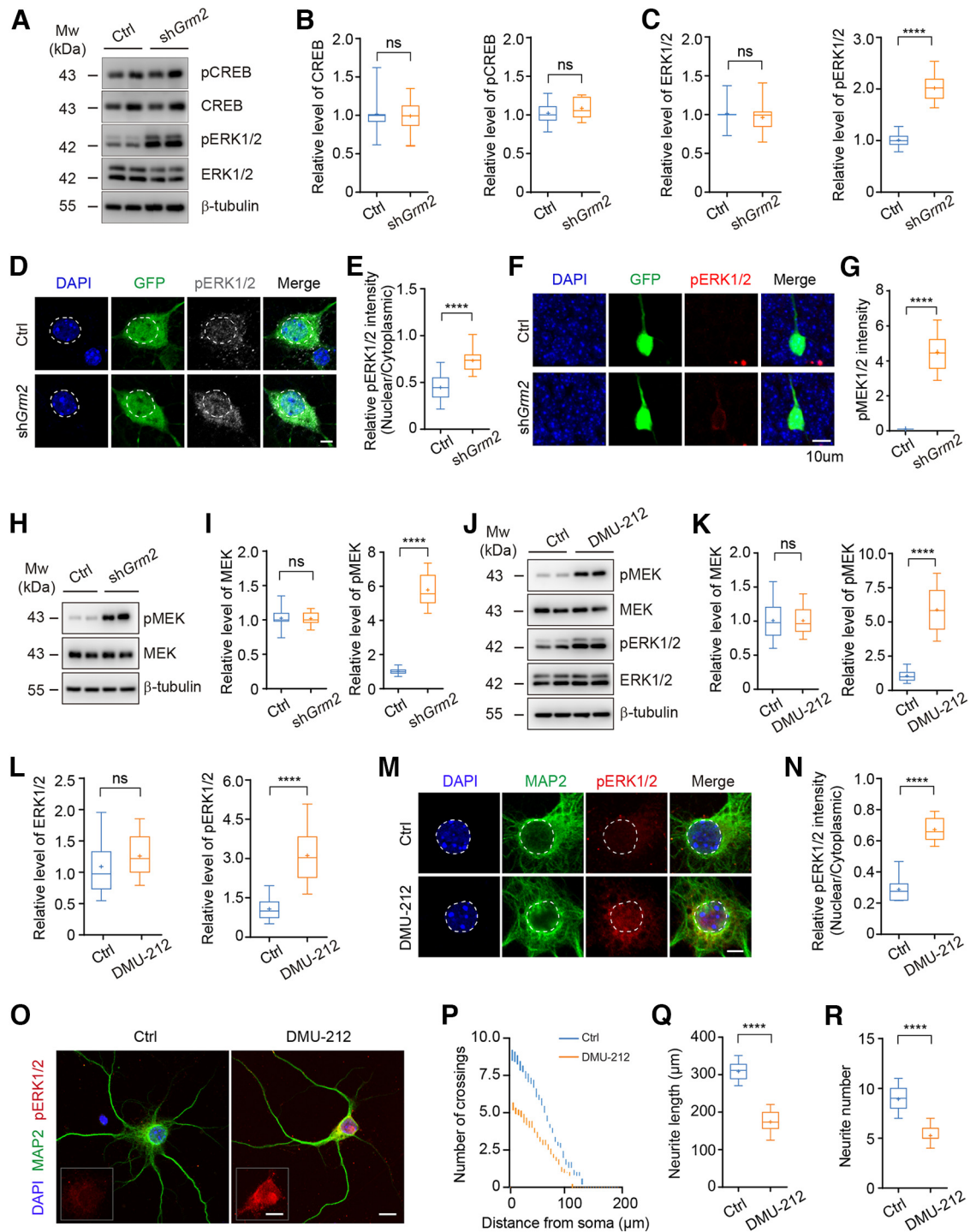


Figure 4. *Grm2* knockdown leads to ERK1/2 phosphorylation and nuclear translocation. **A**, Western blots showing the level of pCREB, CREB, pERK1/2, and total ERK1/2 in cultured hippocampal neurons treated with Ctrl or shGrm2 lentiviruses. **B**, The relative level of total CREB (left) or pCREB (right) were not altered by *Grm2* knockdown (CREB: Ctrl, $n = 8$; shGrm2, $n = 8$; unpaired t test, $t_{(14)} = 0.1996$, $p = 0.8447$; pCREB: Ctrl, $n = 8$; shGrm2, $n = 8$; unpaired t test, $t_{(14)} = 0.8786$, $p = 0.3944$). **C**, *Grm2* knockdown did not change the relative level of total ERK1/2 (left), but increased the level of pERK1/2 (right) in cultured hippocampal neurons (ERK1/2: Ctrl, $n = 12$; shGrm2, $n = 12$; unpaired t test, $t_{(22)} = 0.6396$, $p = 0.529$; pERK1/2: Ctrl, $n = 12$; shGrm2, $n = 12$; unpaired t test, $t_{(22)} = 11.55$, **** $p < 0.0001$). **D**, Images showing *Grm2* knockdown increased pERK1/2 immunofluorescence intensity in cultured hippocampal neurons. Scale bar, 5 μ m. **E**, *Grm2* knockdown increased the relative immunofluorescence intensity of pERK1/2 in the nucleus of cultured hippocampal neurons (Ctrl, $n = 20$ cells; shGrm2, $n = 13$ cells; unpaired t test, $t_{(31)} = 6.308$, **** $p < 0.0001$). **F**, Images showing *Grm2* knockdown increased pERK1/2 immunofluorescence intensity in adult-born DGCs at 3 wpi. Scale bar, 10 μ m. **G**, *Grm2* knockdown increased the relative immunofluorescence intensity of pERK1/2 in adult-born DGCs (Ctrl, $n = 10$ cells; shGrm2, $n = 10$ cells; unpaired t test, $t_{(18)} = 13.42$, **** $p < 0.0001$). **H**, Western blots showing the level of MEK and pMEK in cultured hippocampal neurons treated with Ctrl or shGrm2 lentivirus. **I**, *Grm2* knockdown did not change the level of total MEK (left), but induced an increased level of pMEK in cultured hippocampal neurons (MEK: Ctrl, $n = 10$; shGrm2, $n = 10$; unpaired t test, $t_{(18)} = 0.1393$, $p = 0.8908$; pMEK: Ctrl, $n = 12$; shGrm2, $n = 12$; unpaired t test, $t_{(22)} = 17.64$, **** $p < 0.0001$). **J**, Western blots showing the level of pMEK, total MEK, pERK1/2, and ERK1/2 in cultured hippocampal neurons after DMU-212 treatment. **K**, DMU-212 treatment did not alter the level of total MEK (left), but increased pMEK (right) in cultured hippocampal neurons (MEK: Ctrl, $n = 16$; DMU-212, $n = 16$; unpaired t test, $t_{(30)} = 0.0067$, $p = 0.9947$; pMEK: Ctrl, $n = 16$; DMU-212, $n = 16$; unpaired t test, $t_{(30)} = 11.87$, **** $p < 0.0001$). **L**, DMU-212 treatment did not alter the level of total ERK1/2 (left), but increased pERK1/2 (right) in cultured hippocampal neurons (ERK1/2: Ctrl, $n = 16$; DMU-212, $n = 16$; unpaired t test, $t_{(30)} = 7.6$, **** $p < 0.0001$). **M**, Immunostaining of pERK1/2 in cultured hippocampal neurons after DMU-212 treatment. Scale bar, 5 μ m. **N**, DMU-212 treatment increased

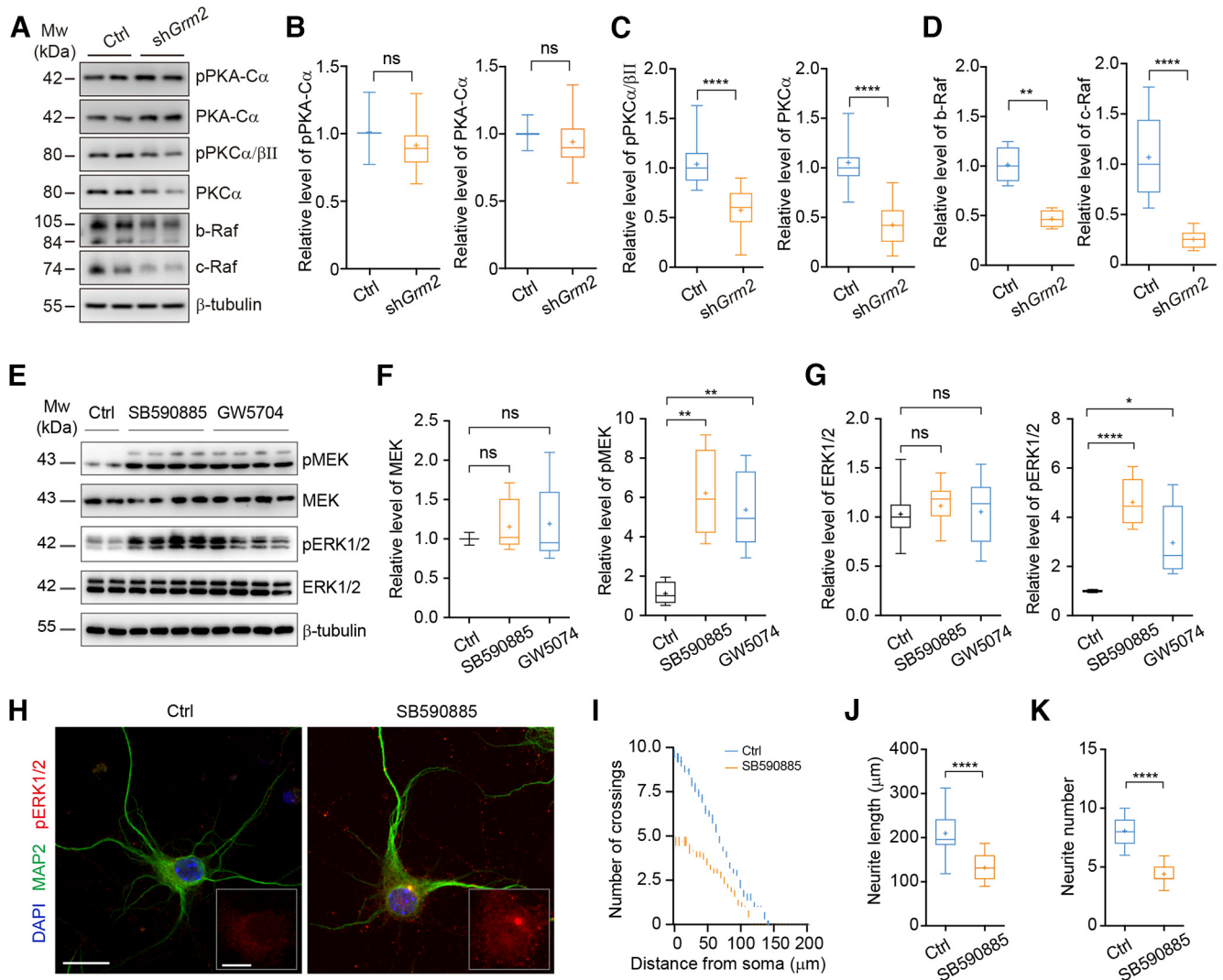


Figure 5. *Grm2* knockdown paradoxically increased MEK/ERK1/2 phosphorylation by inhibiting b/c-Raf. **A**, Western blots showing the changes of the level of pPKA-Cα, total PKA-Cα, pPKCα/βII, total PKCα, b-Raf, and c-Raf in cultured hippocampal neurons after *Grm2* knockdown. **B**, The relative level of pPKA-Cα (left) or total PKA-Cα (right) was not changed in cultured hippocampal neurons after *Grm2* knockdown (pPKA-Cα: Ctrl, *n* = 12; sh*Grm2*, *n* = 12; unpaired *t* test, $t_{(22)} = 1.425$, $p = 0.1681$; PKA-Cα: Ctrl, *n* = 12; sh*Grm2*, *n* = 12; unpaired *t* test, $t_{(22)} = 1.051$, $p = 0.3047$). **C**, The relative level of pPKCα/βII (left) and total PKCα (right) were both decreased in cultured hippocampal neurons after *Grm2* knockdown (pPKCα/βII: Ctrl, *n* = 12; sh*Grm2*, *n* = 12; unpaired *t* test, $t_{(22)} = 5.234$, $****p < 0.0001$; PKCα: Ctrl, *n* = 12; sh*Grm2*, *n* = 12; unpaired *t* test, $t_{(22)} = 6.568$, $****p < 0.0001$). **D**, The relative level of b-Raf (left) and c-Raf (right) were both decreased in cultured hippocampal neurons after *Grm2* knockdown (b-Raf: Ctrl, *n* = 4; sh*Grm2*, *n* = 4; unpaired *t* test, $t_{(6)} = 5.389$, $**p = 0.0017$; c-Raf: Ctrl, *n* = 8; sh*Grm2*, *n* = 8; unpaired *t* test, $t_{(14)} = 5.401$, $****p < 0.0001$). **E**, Western blots showing the level of pMEK, MEK, pERK, and ERK after the treatment of SB590885 or GW5704 in cultured hippocampal neurons. **F**, SB590885 or GW5704 treatment did not change the relative level of total MEK (left: Ctrl, *n* = 8; SB590885, *n* = 16; unpaired *t* test, $t_{(22)} = 1.327$, $p = 0.198$; GW5704, *n* = 16; unpaired *t* test, $t_{(22)} = 1.161$, $p = 0.2582$). Both SB590885 and GW5704 increased pMEK (right: Ctrl, *n* = 4; SB590885, *n* = 8; unpaired *t* test, $t_{(10)} = 4.394$, $**p = 0.0013$; GW5704, *n* = 8; unpaired *t* test, $t_{(10)} = 4.087$, $**p = 0.0022$). **G**, SB590885 or GW5704 treatment did not change the relative level of total ERK (left: Ctrl, *n* = 8; SB590885, *n* = 16; unpaired *t* test, $t_{(22)} = 0.8539$, $p = 0.4023$; GW5704, *n* = 16; unpaired *t* test, $t_{(22)} = 0.1865$, $p = 0.8538$). Both SB590885 and GW5704 increased pERK (right: Ctrl, *n* = 4; SB590885, *n* = 8; unpaired *t* test, $t_{(10)} = 7.312$, $****p < 0.0001$; GW5704, *n* = 8; unpaired *t* test, $t_{(10)} = 2.704$, $*p = 0.0222$). **H**, Representative images showing the morphology of cultured hippocampal neurons treated with SB590885. Scale bar, 20 μm. Insets, Immunofluorescence of pERK1/2. Scale bar, 10 μm. **I**, Sholl analysis of Ctrl and SB590885-treated cultured hippocampal neurons. **J**, SB590885 treatment reduced the neurite length of cultured hippocampal neurons (Ctrl, *n* = 18 cells; SB590885, *n* = 14 cells; unpaired *t* test, $t_{(30)} = 5.341$, $****p < 0.0001$). **K**, SB590885 treatment reduced the neurite number of cultured hippocampal neurons (Ctrl, *n* = 18 cells; SB590885, *n* = 14 cells; unpaired *t* test, $t_{(30)} = 10.32$, $****p < 0.0001$).

←
the relative immunofluorescence intensity of pERK1/2 in the nucleus (Ctrl, *n* = 20 cells; DMU-212, *n* = 13 cells; unpaired *t* test, $t_{(31)} = 14.6$, $****p < 0.0001$). **O**, Representative images showing the morphology of cultured hippocampal neurons treated with DMU-212. Scale bar, 10 μm. Insets, Immunofluorescence of pERK1/2. Scale bar, 5 μm. **P**, Sholl analysis of Ctrl and DMU-212-treated cultured hippocampal neurons. **Q**, DMU-212 treatment reduced the neurite length of cultured hippocampal neurons (Ctrl, *n* = 13 cells; DMU-212, *n* = 15 cells; unpaired *t* test, $t_{(26)} = 13.85$, $****p < 0.0001$). **R**, DMU-212 treatment reduced the neurite number of cultured hippocampal neurons (Ctrl, *n* = 15 cells; DMU-212, *n* = 15 cells; unpaired *t* test, $t_{(28)} = 9.131$, $****p < 0.0001$).

plasticity, we treated the mice with Dox in drinking water from day 7 through day 25 after the last viral injection, while the Ctrl mice were fed with normal drinking water. Approximately 83.78 ± 1.94% of sh*Grm2* neurons (GFP⁺) expressed dTomato in Dox-treated mice, suggesting successful expression of dn*Mapk1* in the majority of newborn neurons infected by sh*Grm2* virus; whereas none of the GFP-labeled newborn DGCs expressed dTomato in Ctrl mice (Fig. 7F,G). We then tested the behaviors of the animals 4 weeks after the last viral injection. We found that the expression of dn*Mapk1* reduced the behavioral deficits of the animals in the novel

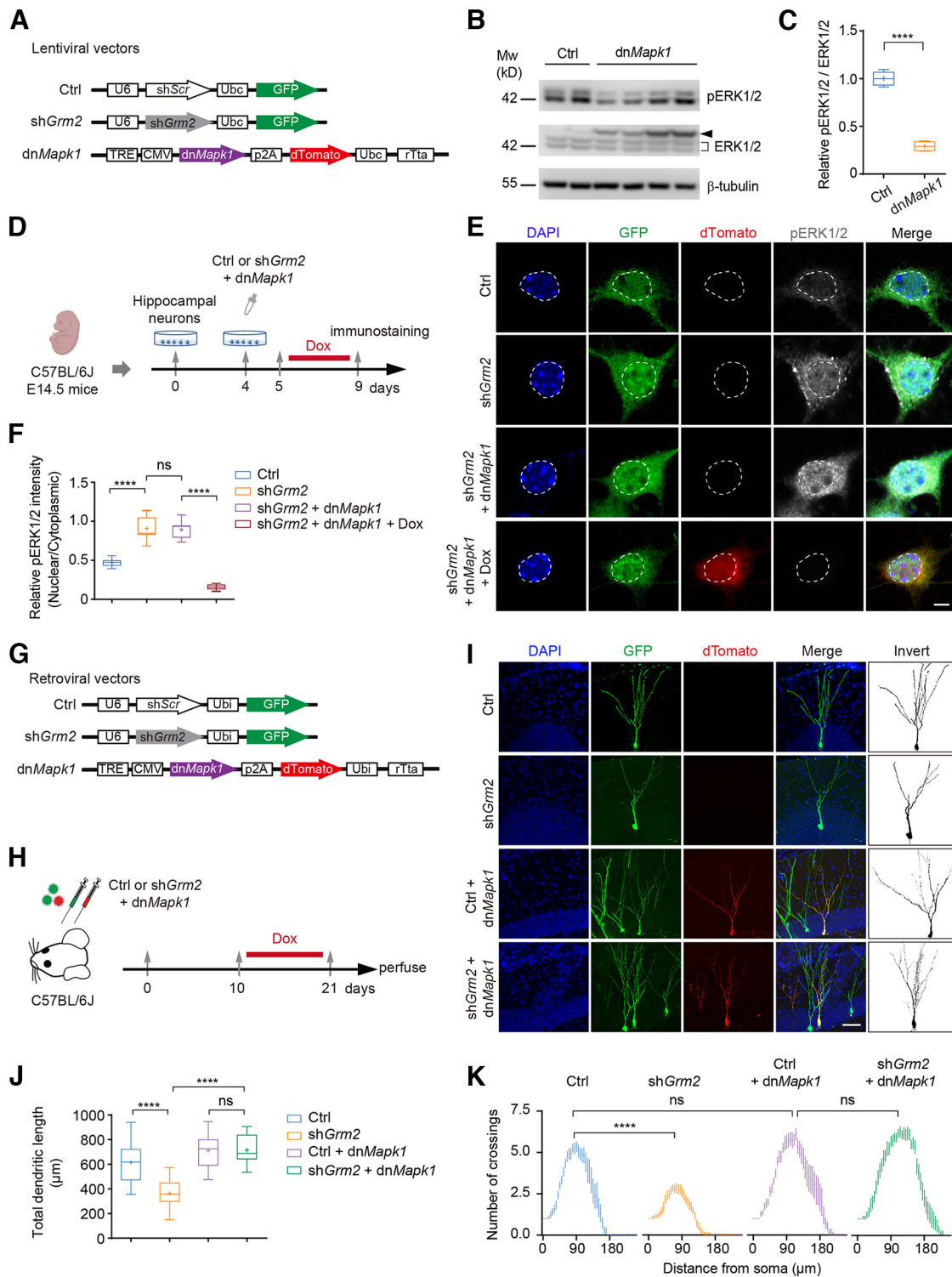


Figure 6. Inhibiting MEK rescues *Grm2* knockdown-induced developmental defects of neurons. **A**, Lentiviral vectors of Ctrl, sh*Grm2*, and dn*Mapk1*. **B**, Western blots showing the level of pERK1/2 and ERK1/2 in cultured hippocampal neurons after Dox-induced expression of dn*Mapk1*. Black arrow indicates the band of the protein product of dn*Mapk1*. **C**, Dox-induced expression of dn*Mapk1* decreased the relative level of pERK1/2 in cultured hippocampal neurons (Ctrl, $n = 8$; dn*Mapk1*/Dox, $n = 8$; unpaired t test, $t_{(14)} = 24.51$, **** $p < 0.0001$). **D**, Schematics showing viral application in cultured hippocampal neurons and the induction of the expression of dn*Mapk1* with Dox. **E**, Confocal images showing Dox-induced expression of dn*Mapk1*-dTomato and pERK1/2 immunofluorescence. Scale bar, 5 μ m. **F**, Expression of dn*Mapk1* prevented *Grm2* knockdown-induced elevation of nuclear level of pERK1/2 (Ctrl, $n = 14$ cells; sh*Grm2*, $n = 15$ cells; sh*Grm2*+dn*Mapk1*, $n = 16$ cells; sh*Grm2*+dn*Mapk1*+Dox, $n = 17$ cells; unpaired t test, Ctrl vs sh*Grm2*: $t_{(27)} = 11.88$, **** $p < 0.0001$; sh*Grm2* vs sh*Grm2*+dn*Mapk1*: $t_{(29)} = 0.3817$, $p = 0.7055$; sh*Grm2*+dn*Mapk1* vs sh*Grm2*+dn*Mapk1*+Dox: $t_{(31)} = 26.42$, **** $p < 0.0001$). **G**, Retroviral vectors of Ctrl, sh*Grm2*, and dn*Mapk1*. **H**, Schematics retroviral injection and Dox treatment. **I**, Representative images showing Dox-induced dn*Mapk1* expression (red) rescued the abnormal development of newborn DGCS caused by *Grm2* knockdown. Scale bar, 50 μ m. **J**, Total dendritic length of virally labeled newborn DGCS at 3 wpi (Ctrl: $N = 3$ mice, $n = 34$ cells; sh*Grm2*: $N = 3$ mice, $n = 26$ cells; Ctrl+dn*Mapk1*: $N = 3$ mice, $n = 13$ cells; sh*Grm2*+dn*Mapk1*: $N = 3$ mice, $n = 18$ cells; unpaired t test; Ctrl vs sh*Grm2*: $t_{(58)} = 6.554$, **** $p < 0.0001$; sh*Grm2* vs sh*Grm2*+dn*Mapk1*: $t_{(42)} = 9.869$, **** $p < 0.0001$; Ctrl+dn*Mapk1* vs sh*Grm2*/dn*Mapk1*: $t_{(29)} = 0.0958$, $p = 0.9243$). **K**, Sholl analysis of the dendritic complexity of newborn DGCS infected by Ctrl, sh*Grm2*, Ctrl+dn*Mapk1*, and sh*Grm2*+dn*Mapk1* viruses, at 3 wpi.

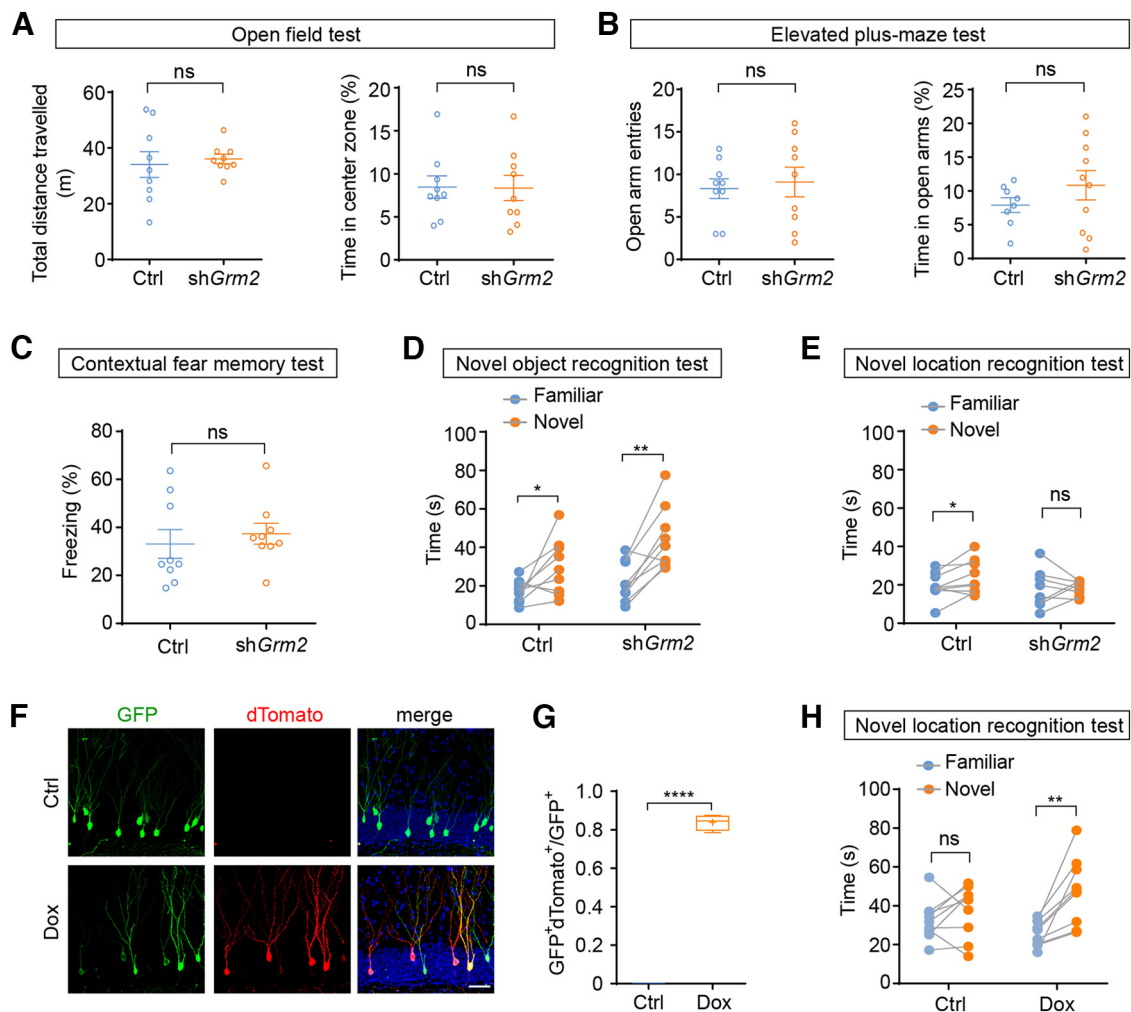


Figure 7. *Grm2* knockdown in adult-born DGCs impaired object-to-place recognition. **A**, Left, The total distance that the animals traveled in the open field test (Ctrl, $N = 9$ mice; shGrm2, $N = 9$ mice; unpaired t test, $t_{(16)} = 0.4053$, $p = 0.6906$). Right, The time that the mice spent in center zone in the open field test (Ctrl, $N = 9$ mice; shGrm2, $N = 9$ mice; unpaired t test, $t_{(16)} = 0.0598$, $p = 0.953$). **B**, Left, The open-arm entries in the elevated plus maze by the mice (Ctrl, $N = 9$ mice; shGrm2, $N = 9$ mice; unpaired t test, $t_{(16)} = 0.3707$, $p = 0.7157$). Right, The time spent in the open arm of the elevated plus maze by the mice (Ctrl, $N = 8$ mice; shGrm2, $N = 10$ mice; unpaired t test, $t_{(16)} = 1.123$, $p = 0.2781$). **C**, The freezing time of the shGrm2 and Ctrl animals during the contextual fear memory test (Ctrl, $N = 9$ mice; shGrm2, $N = 9$ mice; unpaired t test, $t_{(16)} = 0.5805$, $p = 0.5697$). **D**, *Grm2* knockdown did not change the preference of the mice toward the novel object (Ctrl, $N = 9$ mice, paired t test, $t_{(8)} = 2.429$, $*p = 0.0413$; shGrm2: $N = 9$ mice, paired t test, $t_{(8)} = 4.821$, $**p = 0.0013$). **E**, *Grm2* knockdown diminished the preference of the mice toward the object at a novel location (Ctrl: $N = 9$ mice, paired t test, $t_{(8)} = 2.357$, $*p = 0.0462$; shGrm2: $N = 9$ mice, paired t test, $t_{(8)} = 0.9086$, $p = 0.3901$). **F**, Images showing adult-born DGCs labeled by shGrm2 (GFP) and dnMapk1 (dTomato) retroviruses, in Ctrl and Dox-treated mice. Scale bar, 50 μm . **G**, The colocalization of GFP and dTomato in Ctrl and Dox-treated mice (Ctrl, $N = 4$ mice; Dox, $N = 4$ mice; unpaired t test, $t_{(6)} = 43.31$, $****p < 0.0001$). **H**, Expression of dnMapk1 rescued the preference of the mice toward the object at a novel location (Ctrl: $N = 9$ mice, paired t test, $t_{(8)} = 1.076$, $p = 0.3132$; Dox: $N = 9$ mice, paired t test, $t_{(8)} = 4.386$, $**p = 0.0023$).

location recognition test, as the Dox-treated mice showed significant preference toward the novel location, while the Ctrl mice did not (Fig. 7H). These data suggest that suppressing the excessive activation of MEK/ERK1/2 pathway in newborn DGCs lacking GRM2 could restore the physiological functions of these new neurons.

Discussion

GRM2 regulates the development and function of newborn DGCs

Metabotropic glutamate receptors are important for the development and functions of the brain. In the hippocampal DG, group II GRMs, including GRM2 and GRM3, are highly expressed in the granule neurons (Shigemoto et al., 1997). Enriched in the mossy fiber terminals, GRM2 is essential for regulating the synaptic transmission and plasticity of these synapses (Kamiya et al.,

1996; Scanziani et al., 1997; Sanabria et al., 2004; Nicholls et al., 2006), thus regulating hippocampus-related brain functions.

New neurons are continuously generated in the hippocampal DG of adult mammals. After their birth, adult-born neurons gradually acquire the same physiological properties as the existing mature DGCs (Ge et al., 2008). Using retrovirus to specifically date the birth of the newborn neurons, we found that GRM2 expression in the adult-born DGCs was initially low, but gradually increased to a comparable level as in the mature DGCs at 3 weeks of age. Interestingly, knockdown of *Grm2* significantly impaired the development and functional integration of newborn DGCs *in vivo*. For instance, the newborn DGCs with *Grm2* knockdown showed less developed dendrites, fewer dendritic spines, fewer functional synapses formed with afferent axon terminals, and smaller axon boutons connecting with downstream neurons. Similarly, *Grm2* knockdown impaired the growth of cultured hippocampal neurons *in vitro* as well. These data

suggest that GRM2 is required for the normal development of hippocampal neurons. On the other hand, *Grm2* knockdown led to less mature intrinsic electrophysiological properties of the newborn DGCs, suggesting that GRM2 is necessary for the normal neuronal maturation. Additionally, *Grm2* knockdown led to enhanced apoptosis of the newborn DGCs during the third week after their birth, which is a critical time period for their integration. This suggests that GRM2 is important for the circuit integration of the newborn DGCs, and the newborn neurons that failed to integrate because of lack of GRM2 are likely to be cleared by apoptosis.

Moreover, GRM2 mainly locates in the axon terminals of the DGCs (i.e., the MF boutons; Shigemoto et al., 1997), regulating the strength and plasticity of MF synapses (Nicholls et al., 2006). Thus, lack of GRM2 in the newborn DGCs would affect the connectivity and synaptic transmission between DGCs and the downstream target neurons, such as CA3 pyramidal cells and interneurons. Indeed, *Grm2* knockdown led to smaller axon boutons, suggesting impaired connection of these newborn neurons with downstream cellular targets. Functionally, lack of GRM2 in young newborn DGCs may affect the MF synaptic transmission and plasticity, thus ultimately affecting behaviors. We showed that *Grm2* knockdown in a cohort of young newborn DGCs impaired object-to-location recognition, suggesting that GRM2 are important not only for the development of new neurons, but also for their physiological functions.

A previous study has shown that GRM7, one of the group III GRMs, regulates cortical neuronal development via CREB (Xia et al., 2015), which is essential for the development of adult-born hippocampal neurons (Merz et al., 2011). However, we did not find that *Grm2* knockdown alters the level of total CREB or its phosphorylated form. Instead, we found that *Grm2* knockdown led to a significant increase of the phosphorylated forms of MEK and ERK1/2 in developing neurons. Inhibition of MEK by *dnMapk1* could prevent the neuronal developmental defects caused by *Grm2* knockdown, suggesting that proper expression of GRM2 regulates the growth and integration of these neurons by suppressing MEK/ERK1/2 pathway.

MEK/ERK1/2 pathway in regulating neuronal growth

ERK1/2, belonging to the MAPKs family, are important in signal transduction cascades in regulating proliferation, cellular growth, differentiation, and development in various types of cells (Lavoie et al., 2020). When activated by the upstream kinase MEK, phosphorylated ERK1/2 could translocate into the nucleus and subsequently induce the expression of target genes, by activating specific transcription factors either directly or indirectly (Thiels and Klann, 2001; Buscà et al., 2016). In neurons, ERK1/2 signaling is required for the induction of different forms of synaptic plasticity in many brain regions, such as long-term potentiation in hippocampus (Connor et al., 2012; Zhai et al., 2013), striatum (Hawes et al., 2013), and amygdala (Schafe et al., 2008) and long-term depression in cerebellar Purkinje cells (Tanaka and Augustine, 2008).

However, we found that the overactivated ERK1/2 signaling was associated with maldevelopment of neurons *in vitro* and *in vivo*. This is inconsistent with previous findings that sustained activation of the Raf/MEK/ERK pathway induces growth arrest (Hong et al., 2009). With the central role of ERK signaling in brain development, a group of rare developmental syndromes termed “RASopathies” are generally associated with hyperactive ERK signaling (Lavoie et al., 2020). Since ERK1 and ERK2 were both upregulated by *Grm2* knockdown, and ERK1 and ERK2

have redundant roles in mediating MEK/ERK-dependent growth arrest (Hong et al., 2009), we used viral vectors to express a *dnMapk1* to inhibit the catalytic function of MEK, the upstream molecule of the cascade. Our data showed that the inhibition of the aberrantly activated MEK/ERK signaling rescued the neuronal developmental defects caused by *Grm2* knockdown. Consistently, mouse models of RASopathies with brain abnormalities and learning deficits could be rescued by ERK inhibition (Cui et al., 2008; Wang et al., 2012).

Thus, our results suggest that, after the cells choose the neuronal fate, the gradual increase of the expression of GRM2 suppresses the MEK/ERK1/2 signaling, and promotes the development and integration of newborn neurons.

GRM2 paradoxically regulates MEK/ERK1/2 via Raf during neuronal development

As a G-protein-coupled receptor, GRM2 could activate ERK1/2 through second messenger-dependent kinases, such as PKA and PKC, or a β -arrestin-dependent pathway. For example, in Schwann cells, the activation of GRM2 could elicit ERK phosphorylation (Saitoh et al., 2016). In neurons, the activation of GRM2 inhibits cAMP production and PKA activity, thus suppressing transmitter release (Kamiya et al., 1996; Tzounopoulos et al., 1998; Cosgrove et al., 2011). However, in developing neurons, we did not observe the total amount of PKA-C α or phosphorylated PKA-C α that was altered by knockdown of *Grm2*. Instead, we found that knockdown of *Grm2* significantly decreased the total PKC α and the phosphorylated PKC α / β II. Simultaneously, decreased b-Raf and c-Raf were found in the *Grm2* knock-down cells, suggesting an alternative route that GRM2 regulates the Raf/MEK/ERK1/2 pathway. This is inconsistent with previous reports showing that PKC activation could phosphorylate and activate c-Raf through different mechanisms (Corbit et al., 2003; Tanaka and Augustine, 2008), thus the decrease in the activity of PKC resulting in reduced activation of Rafs. In addition, accumulated active MEK/ERK1/2 could suppress b-Raf and c-Raf through a negative feedback loop, which should be considered as well in this scenario.

Interestingly, applying inhibitors of b-Raf or c-Raf on cultured hippocampal neurons elicited the levels of phosphorylated MEK and ERK1/2, and inhibited the development of these neurons. It has been reported that MEK/ERK signaling could be activated by inhibiting b-Raf with a V600E mutation (Holderfield et al., 2014). This paradoxical activation of MEK/ERK1/2 signaling has also been reported by Raf inhibitors on wild-type Raf, possibly by transactivation in homodimerized or heterodimerized b-Raf and c-Raf (Poulikakos et al., 2010; Poulikakos and Rosen, 2011). Therefore, knockdown of *Grm2* in neurons may inhibit Raf kinases by decreasing the activity of PKC, and thus paradoxically elicit the activation of MEK and ERK1/2. As prolonged activation of ERK causes detrimental effects to cells, such as growth arrest (Hong et al., 2009) and apoptosis (Jiang et al., 2018), *Grm2* knockdown led to the maldevelopment of newborn neurons.

Altogether, our data demonstrated that *Grm2* knockdown in newborn DGCs in the adult hippocampus resulted in defects in the development, integration, and functions of these new neurons, through an aberrantly elevated activity of MEK/ERK1/2 signaling. Although cultured hippocampal neurons were mainly pyramidal cells, *Grm2* expression was detected in these cells, while *Grm2* knockdown led to the same phenotype as seen in adult-born DGCs. These suggest that GRM2 expression is necessary for suppressing the MEK/ERK1/2 pathway for the

development and functions of neuronal types that express GRM2. Although the mechanisms determining the activity of Raf kinases and their regulation of MEK/ERK1/2 signaling remain controversial, targeting the MEK/ERK1/2 pathway may be an alternative treatment for disease related to GRM2 deficiency.

References

- Androutsopoulos VP, Fragiadaki I, Tosca A (2015) Activation of ERK1/2 is required for the antimetabolic activity of the resveratrol analogue 3,4,5,4'-tetramethoxystilbene (DMU-212) in human melanoma cells. *Exp Dermatol* 24:632–634.
- Buscà R, Pouysségur J, Lenormand P (2016) ERK1 and ERK2 map kinases: specific roles or functional redundancy? *Front Cell Dev Biol* 4:53.
- Chin PC, Liu L, Morrison BE, Siddiq A, Ratan RR, Bottiglieri T, D'Mello SR (2004) The c-Raf inhibitor GW5074 provides neuroprotection in vitro and in an animal model of neurodegeneration through a MEK-ERK and Akt-independent mechanism. *J Neurochem* 90:595–608.
- Connor SA, Maity S, Roy B, Ali DW, Nguyen PV (2012) Conversion of short-term potentiation to long-term potentiation in mouse CA1 by coactivation of β -adrenergic and muscarinic receptors. *Learn Mem* 19:535–542.
- Corbit KC, Trakul N, Eves EM, Diaz B, Marshall M, Rosner MR (2003) Activation of Raf-1 signaling by protein kinase C through a mechanism involving Raf kinase inhibitory protein. *J Biol Chem* 278:13061–13068.
- Cosgrove KE, Galván EJ, Barrionuevo G, Meriney SD (2011) mGluRs modulate strength and timing of excitatory transmission in hippocampal area CA3. *Mol Neurobiol* 44:93–101.
- Cui Y, Costa RM, Murphy GG, Elgersma Y, Zhu Y, Gutmann DH, Parada LF, Mody I, Silva AJ (2008) Neurofibromin regulation of ERK signaling modulates GABA release and learning. *Cell* 135:549–560.
- Doherty J, Dingleline R (1998) Differential regulation of synaptic inputs to dentate hilar border interneurons by metabotropic glutamate receptors. *J Neurophysiol* 79:2903–2910.
- Duan X, Chang JH, Ge S, Faulkner RL, Kim JY, Kitabatake Y, Liu XB, Yang CH, Jordan JD, Ma DK, Liu CY, Ganesan S, Cheng HJ, Ming GL, Lu B, Song H (2007) Disrupted-In-Schizophrenia 1 regulates integration of newly generated neurons in the adult brain. *Cell* 130:1146–1158.
- Ge S, Sailor KA, Ming GL, Song H (2008) Synaptic integration and plasticity of new neurons in the adult hippocampus. *J Physiol* 586:3759–3765.
- Gonçalves JT, Schafer ST, Gage FH (2016) Adult neurogenesis in the hippocampus: from stem cells to behavior. *Cell* 167:897–914.
- Gu Y, Arruda-Carvalho M, Wang J, Janoschka SR, Josselyn SA, Frankland PW, Ge S (2012) Optical controlling reveals time-dependent roles for adult-born dentate granule cells. *Nat Neurosci* 15:1700–1706.
- Hawes SL, Gillani F, Evans RC, Benkert EA, Blackwell KT (2013) Sensitivity to theta-burst timing permits LTP in dorsal striatal adult brain slice. *J Neurophysiol* 110:2027–2036.
- Holderfield M, Deuker MM, McCormick F, McMahon M (2014) Targeting RAF kinases for cancer therapy: BRAF-mutated melanoma and beyond. *Nat Rev Cancer* 14:455–467.
- Hong SK, Yoon S, Moelling C, Arthan D, Park JI (2009) Noncatalytic function of ERK1/2 can promote Raf/MEK/ERK-mediated growth arrest signaling. *J Biol Chem* 284:33006–33018.
- Hu Z, Ma J, Yue H, Luo Y, Li X, Wang C, Wang L, Sun B, Chen Z, Wang L, Gu Y (2022) Involvement of LIN28A in Wnt-dependent regulation of hippocampal neurogenesis in the aging brain. *Stem Cell Rep* 17:1666–1682.
- Jiang S, Li X, Jin W, Duan X, Bo L, Wu J, Zhang R, Wang Y, Kang R, Huang L (2018) Ketamine-induced neurotoxicity blocked by *N*-Methyl-D-aspartate is mediated through activation of PKC/ERK pathway in developing hippocampal neurons. *Neurosci Lett* 673:122–131.
- Jin T, Lavoie H, Sahmi M, David M, Hilt C, Hammell A, Therrien M (2017) RAF inhibitors promote RAS-RAF interaction by allosterically disrupting RAF autoinhibition. *Nat Commun* 8:1211.
- Kamiya H, Shinozaki H, Yamamoto C (1996) Activation of metabotropic glutamate receptor type 2/3 suppresses transmission at rat hippocampal mossy fibre synapses. *J Physiol* 493: 447–455.
- Kao S, Jaiswal RK, Kolch W, Landreth GE (2001) Identification of the mechanisms regulating the differential activation of the MAPK cascade by epidermal growth factor and nerve growth factor in PC12 cells. *J Biol Chem* 276:18169–18177.
- Kim JI, Drahushuk KM, Kim WY, Gonsiorek EA, Lein P, Andres DA, Higgins D (2004) Extracellular signal-regulated kinases regulate dendritic growth in rat sympathetic neurons. *J Neurosci* 24:3304–3312.
- Kumamoto N, Gu Y, Wang J, Janoschka S, Takemaru K, Levine J, Ge S (2012) A role for primary cilia in glutamatergic synaptic integration of adult-born neurons. *Nat Neurosci* 15:399–405, S1.
- Lavoie H, Gagnon J, Therrien M (2020) ERK signalling: a master regulator of cell behaviour, life and fate. *Nat Rev Mol Cell Biol* 21:607–632.
- Lee HG, Ogawa O, Zhu X, O'Neill MJ, Petersen RB, Castellani RJ, Ghanbari H, Perry G, Smith MA (2004) Aberrant expression of metabotropic glutamate receptor 2 in the vulnerable neurons of Alzheimer's disease. *Acta Neuropathol* 107:365–371.
- Lybrand ZR, Goswami S, Zhu J, Jarzabek V, Merlock N, Aktar M, Smith C, Zhang L, Varma P, Cho KO, Ge S, Hsieh J (2021) A critical period of neuronal activity results in aberrant neurogenesis rewiring hippocampal circuitry in a mouse model of epilepsy. *Nat Commun* 12:1423.
- Maccaferri G, Tóth K, McBain CJ (1998) Target-specific expression of presynaptic mossy fiber plasticity. *Science* 279:1368–1370.
- Merz K, Herold S, Lie DC (2011) CREB in adult neurogenesis—master and partner in the development of adult-born neurons? *Eur J Neurosci* 33:1078–1086.
- Nicholls RE, Zhang XL, Bailey CP, Conklin BR, Kandel ER, Stanton PK (2006) mGluR2 acts through inhibitory G alpha subunits to regulate transmission and long-term plasticity at hippocampal mossy fiber-CA3 synapses. *Proc Natl Acad Sci U S A* 103:6380–6385.
- Pacheco Ojalora LF, Couoh J, Shigemoto R, Zarei MM, Garrido Sanabria ER (2006) Abnormal mGluR2/3 expression in the perforant path termination zones and mossy fibers of chronically epileptic rats. *Brain Res* 1098:170–185.
- Poulikakos PI, Rosen N (2011) Mutant BRAF melanomas—dependence and resistance. *Cancer Cell* 19:11–15.
- Poulikakos PI, Zhang C, Bollag G, Shokat KM, Rosen N (2010) RAF inhibitors transactivate RAF dimers and ERK signalling in cells with wild-type BRAF. *Nature* 464:427–430.
- Saitoh F, Wakatsuki S, Tokunaga S, Fujieda H, Araki T (2016) Glutamate signals through mGluR2 to control Schwann cell differentiation and proliferation. *Sci Rep* 6:29856.
- Sanabria ER, Wozniak KM, Slusher BS, Keller A (2004) GCP II (NAALADase) inhibition suppresses mossy fiber-CA3 synaptic neurotransmission by a presynaptic mechanism. *J Neurophysiol* 91:182–193.
- Scanziani M, Salin PA, Vogt KE, Malenka RC, Nicoll RA (1997) Use-dependent increases in glutamate concentration activate presynaptic metabotropic glutamate receptors. *Nature* 385:630–634.
- Schafe GE, Swank MW, Rodrigues SM, Debiec J, Doyère V (2008) Phosphorylation of ERK/MAP kinase is required for long-term potentiation in anatomically restricted regions of the lateral amygdala in vivo. *Learn Mem* 15:55–62.
- Shigemoto R, Kinoshita A, Wada E, Nomura S, Ohishi H, Takada M, Flor PJ, Neki A, Abe T, Nakanishi S, Mizuno N (1997) Differential presynaptic localization of metabotropic glutamate receptor subtypes in the rat hippocampus. *J Neurosci* 17:7503–7522.
- Sun B, Halabisky B, Zhou Y, Palop JJ, Yu G, Mucke L, Gan L (2009) Imbalance between GABAergic and glutamatergic transmission impairs adult neurogenesis in an animal model of Alzheimer's disease. *Cell Stem Cell* 5:624–633.
- Tanaka K, Augustine GJ (2008) A positive feedback signal transduction loop determines timing of cerebellar long-term depression. *Neuron* 59:608–620.
- Thiels E, Klann E (2001) Extracellular signal-regulated kinase, synaptic plasticity, and memory. *Rev Neurosci* 12:327–345.
- Toni N, Laplagne DA, Zhao C, Lombardi G, Ribak CE, Gage FH, Schinder AF (2008) Neurons born in the adult dentate gyrus form functional synapses with target cells. *Nat Neurosci* 11:901–907.

- Tsao HK, Chiu PH, Sun SH (2013) PKC-dependent ERK phosphorylation is essential for P2X7 receptor-mediated neuronal differentiation of neural progenitor cells. *Cell Death Dis* 4:e751.
- Tzounopoulos T, Janz R, Südhof TC, Nicoll RA, Malenka RC (1998) A role for cAMP in long-term depression at hippocampal mossy fiber synapses. *Neuron* 21:837–845.
- Walter C, Murphy BL, Pun RY, Spieles-Engemann AL, Danzer SC (2007) Pilocarpine-induced seizures cause selective time-dependent changes to adult-generated hippocampal dentate granule cells. *J Neurosci* 27:7541–7552.
- Wang JQ, Mao L (2019) The ERK pathway: molecular mechanisms and treatment of depression. *Mol Neurobiol* 56:6197–6205.
- Wang Y, Kim E, Wang X, Novitsch BG, Yoshikawa K, Chang LS, Zhu Y (2012) ERK inhibition rescues defects in fate specification of Nf1-deficient neural progenitors and brain abnormalities. *Cell* 150:816–830.
- Xia W, Liu Y, Jiao J (2015) GRM7 regulates embryonic neurogenesis via CREB and YAP. *Stem Cell Rep* 4:795–810.
- Yokoi M, Kobayashi K, Manabe T, Takahashi T, Sakaguchi I, Katsuura G, Shigemoto R, Ohishi H, Nomura S, Nakamura K, Nakao K, Katsuki M, Nakanishi S (1996) Impairment of hippocampal mossy fiber LTD in mice lacking mGluR2. *Science* 273:645–647.
- Zhai S, Ark ED, Parra-Bueno P, Yasuda R (2013) Long-distance integration of nuclear ERK signaling triggered by activation of a few dendritic spines. *Science* 342:1107–1111.